Solvent Composition and Viscosity Effects on the Kinetics of CO Binding to Horse Myoglobin †

ARTICLE *in* BIOCHEMISTRY · FEBRUARY 1998

Impact Factor: 3.02 · DOI: 10.1021/bi971508q · Source: PubMed

6 AUTHORS, INCLUDING:

Wolfgang Doster
Technische Universität München
64 PUBLICATIONS **3,452** CITATIONS

SEE PROFILE

Solvent Composition and Viscosity Effects on the Kinetics of CO Binding to Horse Myoglobin†

Thomas Kleinert, Wolfgang Doster,* Harald Leyser, Winfried Petry, Veronika Schwarz,‡ and Marcus Settles§

Technische Universität München, Physik-Department E13, D-85747 Garching, Germany

Received June 23, 1997; Revised Manuscript Received October 22, 1997⊗

ABSTRACT: Ligand binding to myoglobin in aqueous solution involves two kinetic components, one extramolecular and one intramolecular, which have been interpreted in terms of two sequential kinetic barriers. In mixed solvents and sub-zero temperatures, the outer barrier increases and the inner barrier splits into several components, giving rise to fast intramolecular recombination. The nature of these barriers and their relation to structural relaxation are examined using the effect of solvent composition and viscosity on the kinetics of CO binding to horse myoglobin in 60% ethylene glycol/water, 75% and 90% glycerol/water, 80% and 92% sucrose/water solutions. Measurements of the corresponding solvent structural relaxation rates by frequency resolved calorimetry allow us to discriminate between solvent composition and viscosity-related effects. The outer kinetic barrier controlling ligand entry and release depends on the viscosity consistent with Kramers−Stokes law of activated escape in the presence of friction. At high cosolvent concentration, we observe deviations from Stokes law, implying a smaller microviscosity at the protein−solvent interface as compared to the bulk. The inner barrier and its coupling to structural relaxation appears to be independent of viscosity but changes with solvent composition. As a possible explanation, we discuss the role of distal water molecules in the formation of the effective inner barrier. At low temperatures, this barrier has a distributed height, depending only slightly on the nature of the cosolvent and temperature at low cosolvent concentrations. In contrast, myoglobin embedded in a sucrose glass (92% sucrose/water) exhibits a temperature-dependent and bimodal enthalpy distribution. This result demonstrates that the exchange between protonation states of His64, $A_0 \leftrightarrow A_1$, can take place in the glass and at temperatures as low as 80 K.

The association−dissociation reaction of myoglobin (Mb)[1] with dioxygen (O_2) or carbon monoxide (CO) has been characterized in terms of an outer and an inner kinetic barrier (Doster et al., 1982; Carver et al., 1990; Steinbach et al., 1991). The outer kinetic barrier for entry into myoglobin and the inner barrier for rebinding from within the heme pocket are believed to be of similar height for O_2. The inner kinetic barrier for CO binding, in contrast, is much larger than the outer barrier and controls the overall association rate λ_S (Doster et al., 1982). In the latter case, one can view the association reaction as a fast preequilibrium between the intramolecular ligand position C and the dissociated state S in sequence with the bond formation of CO with the heme iron, leading to the bound state A:

$$A \leftarrow C \rightleftharpoons S \tag{1}$$

By flash photolysis, one prepares the system in state C initially, in contrast to S in a stopped-flow experiment. From C, the ligand either rebinds directly or, depending on the relative height of the outer and inner barrier, escapes to the solvent. The association rate at excess ligand concentrations, $S \rightarrow A$, can be written as the product of the bond formation rate k_{CA}, the equilibrium constant of $C \rightleftharpoons S$, and the fraction N_S of molecules where the ligand escapes to the solvent (Doster et al., 1982):

$$\lambda_S = k_{CA} P_C N_S \tag{2}$$

with

$$P_C = \frac{k_{SC}}{k_{CS}}$$

$$N_S = \frac{k_{CS}}{k_{CS} + k_{CA}}$$

The factor $N_S \leq 1$ corrects for the fact that the preequilibrium may not be established on a time scale much faster than $1/k_{CA}$. For CO binding in water at room temperature the escape fraction N_S equals 0.96 (Henry et al., 1983) because

† This work was supported in part by the Deutsche Forschungsgemeinschaft (Grant Do 241/2-1) and by the EC-Network on Protein Function and Dynamics.

* To whom correspondence should be addressed.

‡ Present address: Institut für Physikalische Chemie, Ludwig-Maximilians-Universität München, D-80333 München, Germany.

§ Present address: Institut für Röntgendiagnostik, Klinikum Rechts der Isar, D-81675 München, Germany.

⊗ Abstract published in *Advance ACS Abstracts,* December 15, 1997.

[1] Abbreviations: Mb, myoglobin; hMb, horse skeletal myoglobin; swMb, sperm whale myoglobin; MbCO, carbon monoxymyoglobin; E/W, ethylene glycol/water; G/W, glycerol/water; S/W, sucrose/water.

S0006-2960(97)01508-0 CCC: $15.00
Published on Web 01/13/1998

of the large inner barrier. For quasi-physiological sample conditions, this model works quite well. However, kinetic experiments performed at lower temperatures or using high viscosity solvents reveal a surprising complexity of the inner barrier: The intramolecular rebinding phase splits into several components, which, according to their kinetic shape, contain further subcomponents (Austin et al., 1975). This behavior supposedly reflects the hierarchy of conformational substates and represents an important aspect of protein function according to Frauenfelder (1997). The question of whether the additional barriers are low-temperature- or viscosity-induced effects (Ansari et al., 1992) or if low-temperature experiments reveal relevant mechanistic details that are blurred in the physiological range is still open: In simple terms, two types of modifications of eq 1 have been proposed in order to account for the extended range experiments. Some workers complement C by further intramolecular kinetic states B and D (Austin et al., 1975; Doster et al., 1982; Lambright et al., 1993; Ansari et al., 1994). Since the capital letters denote ligand positions, it is implied that B or D denote altered locations or orientations of the ligand in the protein relative to C. Interestingly, CO recombination requires two further intermediates (B and D), while one is sufficient (B) for dioxygen binding (Steinbach et al., 1991). The innermost barrier controlling the final step B → A can be characterized in low-temperature experiments, where the population of other intermediates remains negligible. The extrapolation of the low-temperature kinetic analysis to physiological conditions, however, leads to discrepancies with experimental results (Henry et al., 1983). The inner barrier appears to be much larger than inferred from low temperature work. A pure sequential kinetic scheme is therefore inconsistent with experimental data. Some authors thus introduce an ensemble of sequential kinetic schemes, one for each protein conformation. Structural relaxation is then assumed to induce transitions between pathways resulting effectively in a directed pathway model (Lambright et al., 1993; Ansari et al., 1994; Hagen et al., 1996). Such a description accounts naturally for the observed polychromatic kinetic curves but has the drawback of complexity. Little is known about the number of kinetically relevant pathways and the inter-pathway transition rates.

The second approach is based on a time-dependent sequential scheme (Steinbach et al., 1991). The idea of relaxation-induced barrier increase, originally described by Agmon and Hopfield (1983), has been extended and modified by several groups (Steinbach et al., 1991; Srajer & Champion, 1991; Agmon & Sastry, 1996). Instead of introducing new intermediates, all the complexity is put into protein-coupled barrier changes, which leaves eq 1 denoting ligand positions unchanged. Since one cannot exclude that structural relaxation and ligand displacement are coupled, we use instead of eq 1 a directed pathway model, where horizontal steps indicate ligand displacements while steps along the vertical axis denote conformational changes:

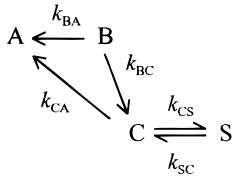

(3)

The C → A and the B → C transitions are supposed to be diagonal, involving both structural change and ligand adjustment. In a sequential kinetic scheme, association and dissociation proceed along the same pathway. The relaxation model in contrast, implies a directed pathway. Dissociation proceeds via the unrelaxed B intermediate, but association from S involves the direct process C → A with $k_{CB} = 0$. This difference has important consequences on the interpretation of ligand binding at physiological conditions. In the latter case, the B → A barrier, which is seen at low temperatures, is of no concern at high temperature. Instead the C → A barrier controls the overall CO association rate.

The goal of our study was to investigate the nature of the inner and outer barriers using viscosity and cosolvent concentration as the parameters discriminating between intramolecular and surface-coupled processes. Protein relaxation was shown to depend on the bulk viscosity of the solvent (Ansari et al., 1992, 1994), which was reported to be frozen-in when myoglobin is embedded in a trehalose glass (Hagen et al., 1995; 1996). Similar results were discussed by Gottfried et al. (1996) for human hemoglobin in a trehalose glass where the high viscosity of the solvent reduces structural motions of the F-helix, which are supposedly involved in protein relaxation. If this relaxation process is the one that is kinetically relevant one expects B → C to depend on the viscosity. The viscosity can be changed by many orders in magnitude by choosing glass-forming solvents that differ in their glass temperature. The effective activation energy of the viscosity close to the glass transition generally exceeds 80 kJ/mol, which is larger than most protein-intrinsic kinetic barriers. The viscosity thus dominates the temperature dependence of surface-coupled kinetic rate coefficients, which is easily detected. Studies performed at constant temperature and variable solvent composition have the drawback that two unrelated parameters, viscosity and composition, are modified simultaneously. The effect of solvent composition on the kinetics of ligand binding has received little attention. The cosolvent modifies the dielectric constant, the chemical potential of water, and the surface tension at the protein−solvent interface. The latter may lead to partial demixing and enhanced concentration of one component in the vicinity of the protein. Two well-known protein stabilizers, glycerol and sucrose, increase the surface tension, which causes exclusion of the cosolvent from the protein domain (Timasheff, 1993). The resulting preferential hydration may reduce the microviscosity near the protein surface relative to the bulk. Moreover, the osmotic stress imposed by high cosolvent concentrations to accumulate water at the interface may also affect the population of protein-internal water molecules. Mutant studies with myoglobin indicate that the removal of a water molecule from the distal pocket of deoxy-myoglobin plays an important role in determining the association rate coefficient (Cameron et al., 1993; Quillin et al., 1995). This suggests that the stability of intermediate C may depend on the solvent composition. The correlation between water activity, protein hydration, conformational equilibria, and ligand binding was investigated previously using high concentrations of organic cosolvents (Cupane et al., 1986; Bulone et al., 1991; Colombo et al., 1992; Rand, 1992; Rand et al., 1993).

The classical case of diffusion-limited association leads to rates that scale with the inverse power of the viscosity:

$\lambda_S \propto 1/\eta$. The association rates of CO and O_2 with heme proteins, myoglobin, hemerythrin, and microperoxidase (Ansari et al., 1992; Hasinoff, 1981; Lavalette & Tetreau, 1988) show this behavior for large η but tend to a finite limit at low viscosity. This result was interpreted in terms of a transition from diffusion to barrier-controlled association. Diffusion in sequence with barrier crossing leads to the following association rate constant (Noyes, 1961):

$$\lambda_S^{-1} = k_{Barr}^{-1} + k_{Diff}^{-1} \qquad k_{Diff} = 4\pi Dr \tag{4}$$

D denotes the sum of the diffusion coefficients and r is the combined encounter radius of two associating molecules. k_{Barr} is the rate of barrier crossing. Since $D \propto 1/\eta$, eq 4 yields

$$\lambda_S \propto 1/(c + \eta) \tag{5}$$

c refers to a viscosity-independent constant. However, the observation of a viscosity-dependent rate coefficient alone does not prove the relevance of translational diffusion. For instance, the rate of a conformational transition induced by photolysis of MbCO was interpreted using eq 5 (Ansari et al., 1992; 1994). The authors assign the constant $c = \eta_0$ to a protein internal viscosity. Furthermore, the Frauenfelder group has shown that not only the association process of ligands with myoglobin but also dissociation depends on the external viscosity (Beece et al., 1980). In terms of eqs 1 and 2, this result implies that both rate coefficients, k_{SC} and k_{CS}, and thus the effective height of the outer barrier depends on the viscosity of the solvent. The case of barrier crossing in the presence of friction was treated by Kramers (1940). In the high damping limit, one obtains a modified transition state result, where the preexponential varies inversely proportional with the friction coefficient, f:

$$k_{ij} = \frac{\omega_1\omega_2}{2\pi f} \exp\left(-\frac{H_{ij}}{RT}\right) \tag{6}$$

H_{ij} denotes the activation enthalpy of the transition $i \rightarrow j$; ω_1, ω_2 are the harmonic frequencies near the bottom and top of the barrier. According to Stokes law, one should expect $f \propto \eta$, which gives $k_{ij} \propto 1/\eta$. However, this simple behavior is rarely seen with protein reactions. Several groups have studied solvent viscosity effects on protein reactions (Gavish & Werber, 1979; Beece et al., 1980, 1981; Lavalette & Tetreau, 1988; Rosenberg et al., 1989; Ng & Rosenberg, 1991; Doster et al., 1995; Yedgar et al., 1995) and on reorientation of spin-labels bound to protein surfaces (Steinhoff, 1990). In all cases, except for the conformational change mentioned above (Ansari et al., 1992), the interconversion rates of the transition between taxonomic substates (Tian et al., 1996) and the catalytic rate of carboxy peptidase (Gavish & Werber, 1979), a fractional power law in the viscosity was observed: $k_{ij} \propto \eta^{-\kappa}$, $\kappa \leq 1$. Furthermore, a kinetic analysis of CO binding to sperm whale myoglobin leads to transition rates that tend to a finite limit at extreme viscosities (Beece et al., 1980) suggesting instead of eq 5

$$k_{ij} \propto C_1 + \frac{C_2}{\eta^{\kappa}} \tag{7}$$

Equation 7 predicts the decoupling of structural motion from the solvent at high viscosity. This result is at variance with experiments on myoglobin, which indicate that protein flexibility vanishes in parallel with the glass transition of the solvent (Iben et al., 1989). At present there is no general agreement on the meaning of fractional exponents implying a breakdown of Stokes law, $f \propto \eta$. A recent kinetic study on oxygen binding to hemerythrin has shown that κ depends on the molecular weight of the cosolvent used to change the viscosity (Yedgar et al., 1995). Theoretical studies suggest either position-dependent (Gavish, 1980) or frequency-dependent friction coefficients (Doster, 1983; Schlitter, 1988). In the following, we investigate these questions with horse myoglobin, which has a simpler kinetic structure than the sperm whale species (Post et al., 1993). As solvents, we choose 60% ethylene glycol/water, 75% and 90% glycerol/water, 80% and 92% sucrose/water to cover a wide range of viscosity according to glass temperatures from 140 K (60% E/W) to 277 K (92% S/W). Also, we measure the viscosity and structural relaxation time of the solvent using specific heat spectroscopy. This allows us to study viscosity effects by varying the temperature at fixed solvent composition and to discriminate viscosity from solvent composition-induced effects.

MATERIALS AND METHODS

Sample Preparation. Glycerol/water and ethylene glycol/water solvents were adjusted at pH 7.6 by adding 0.1 M phosphate buffer. To avoid crystallization, the sucrose was dissolved in an excess of water at a temperature of 70 °C and then cooled to 50 °C. Subsequently, the water was removed by evacuating the flask containing the mixture until a weight concentration of 80% was reached. The concentration was measured by weighing the solution and comparing its weight to the weight of the empty flask and the sucrose. All solvents were equilibrated with carbon monoxide (CO) at 1 atm. For 80% sucrose/water, we determined the calorimetric glass transition at 227 ± 3 K using differential scanning calorimetry (Perkin Elmer, scanning rate 8 K/min).

For flash photolysis experiments, the samples were prepared from salt-free lyophilized powder of horse skeletal metmyoglobin (Sigma Chemie, Germany). The material was dissolved at a concentration of 0.6 mM in the corresponding solvent. After equilibration with CO at 1 atm, the protein was reduced by adding a 10-fold excess of sodium dithionite under anaerobic conditions. Due to the high viscosity of 80% sucrose/water, it was not possible to dissolve the protein at room temperature. Therefore, we added a 3 mM MbCO/water solution (pH 7) at 50 °C to the sucrose/water solution. The excess water was removed by evaporation, and the solution was immediately cooled to 0 °C. After preparation, all samples had protein concentrations near 0.6 mM at pH 7, and the optical absorption spectra were identical with those observed for aqueous hMbCO.

For the 92% sucrose/water sample, we used a 0.3 mM MbCO/water solution that contained 50 mM sucrose. A quantity of 125 μL was dried on a quartz plate in a desiccator filled with silica gel for several days. The desiccator was flooded with CO and kept at 5 °C during dehydration. This preparation yielded an optically homogeneous film with an extinction of ≈1.2 at the Soret peak (424 nm) and an estimated thickness of 40 ± 10 μm. For a determination of the residual water after dehydration, we dried a 50-fold

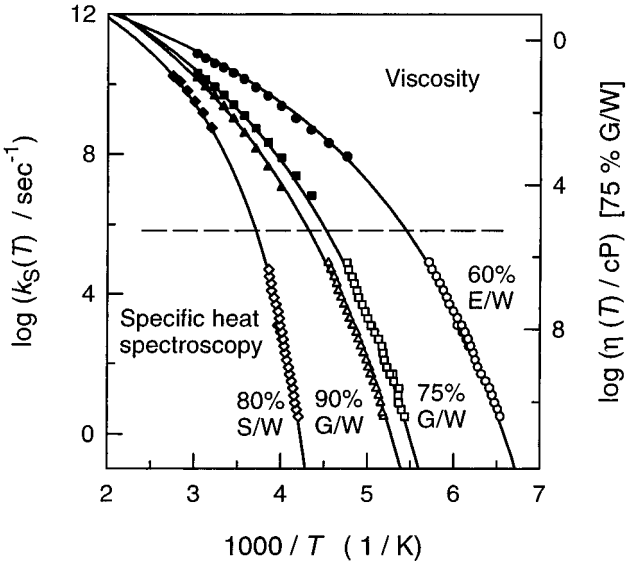

FIGURE 1: Solvent relaxation rates $k_S(T)$ measured with specific heat spectroscopy (open symbols) and viscosity data (closed symbols, Nikolski, 1959; Douzou, 1977; Hasinoff, 1977; Beece et al., 1980) for 60% ethylene glycol/water, 75% and 90% glycerol/water, and 80% sucrose/water (from the right to the left) in an Arrhenius plot (log values here and in the following text and figures are base 10). Lines represent fits using the Vogel−Fulcher−Tamman eq 9. The right-hand axis for viscosity refers to 75% glycerol/water only. The high frequency moduli G_∞ in eq 8 of the various solvents differ slightly. By eqs 8 and 9 and the data of Table 1, one obtains the viscosity values of the other solvents.

amount of the myoglobin/sucrose/water solution in the same way and calculated from the weight of the dehydrated sample in comparison to the weight of myoglobin, sucrose, and buffer salts a final ratio of 92 ± 2% (w/w) sucrose to water. Using differential scanning calorimetry (Rheometric Scientific, scanning rate 10 K/min), we measured the glass transition at a temperature T_g of 277 ± 3 K and the onset of protein denaturation at ≈ 104 °C. T_g exactly matches the curve of glass transition temperatures for sucrose/water mixtures published by Crowe and co-workers (Sun et al., 1996; Crowe et al., 1996).

We performed the specific heat experiments with 60% ethylene glycol/water, 75% and 90% glycerol/water, and 80% sucrose/water solvents. The addition of protein had no measurable effect on the results.

Specific Heat Spectroscopy. The specific heat, usually known to be static, becomes time-dependent if some degrees of freedom show relaxation behavior. In supercooled liquids, diffusive motions of the molecules slow down with temperature, and their characteristic time scale exceeds the experimental time scale at the glass transition temperature. These structural relaxations give an additional contribution to the vibrational part of the specific heat. The mean relaxation time τ_S at a particular temperature can be determined from a frequency-dependent measurement of the specific heat. The method of specific heat spectroscopy (Birge & Nagel, 1985; Birge, 1986) has been described in a previous publication (Settles et al., 1992). The principle is as follows: A modulated heat source induces a small temperature oscillation ($\Delta T \approx 100$ mK) in the sample due to linear response theory (Kubo, 1957). The temperature oscillation defines a complex specific heat at constant pressure. Amplitude and phase of the oscillation are measured using lock-in technique. If the frequency of the heat source exceeds the inverse structural relaxation time, the transfered heat is no longer absorbed by the structural degrees of freedom. This leads to increased temperature oscillations in the heat source and to a phase shift. This transition, which depends on the temperature and the frequency of the heat oscillation, is used to determine the structural relaxation time of the solvent. An Arrhenius plot of the resulting structural relaxation rates, $k_S = 1/\tau_S$, of 60% ethylene glycol/water, 75% and 90% glycerol/water, and 80% sucrose/water is given in Figure 1.

Table 1: Parameters of Vogel−Fulcher−Tamman Fits eq 9 and g_∞ for 60% Ethylene Glycol/Water, 75% and 90% Glycerol/Water, and 80% Sucrose/Water

solvent	log τ_{vft} (s)	A_{vft} (K)	T_{vft} (K)	log g_∞ (cP K^{-1} s^{-1})
60% E/W	−12.8 ± 0.7	1200 ± 150	110 ± 3	8.2±0.4
75% G/W	−14.2 ± 0.4	1850 ± 100	125 ± 3	8.6 ± 0.3
90% G/W	−15.3 ± 0.5	2300 ± 100	125 ± 3	9.6 ± 0.3
80% S/W	−13.6 ± 0.4	1450 ± 50	190 ± 3	9.2 ± 0.3

The Maxwell relation (Scherer, 1986) connects the structural relaxation time to the bulk viscosity, η. It involves the high frequency shear modulus G_∞:

$$\eta = G_\infty \tau_S = \frac{G_\infty}{k_S} \tag{8}$$

Equation 8 allows us to extend the dynamic range of the specific heat experiments using published viscosity data (Nikolski, 1959; Douzou, 1977; Hasinoff, 1977; Beece et al., 1980). We determine the shear modulus in a region where both viscosity and relaxation times are available. Figure 1 shows that the relaxation rates (open symbols) and viscosities (closed symbols) of the mixed solvents are well approximated by a Vogel−Fulcher−Tamman (VFT) equation (solid lines):

$$\tau_S(T) = \tau_{vft} \exp \frac{A_{vft}}{T - T_{vft}} \tag{9}$$

In Table 1, we summarize the parameters of eqs 8 and 9 for different solvents, with $G_\infty = g_\infty T$ (Schofield, 1966).

Flash Photolysis. Photolysis of the CO-ligated ensemble was achieved by a 7-ns pulse of a frequency-doubled Nd:YAG Laser (Spectra Physics DCR 11) with a pulse energy of 80 mJ at the sample. To avoid photoselection, the laser beam was depolarized by a turbid glass plate. The extinction change of the sample after photolysis was monitored using a time-resolving transmission spectrometer. The spectrometer consists of a stabilized quartz tungsten lamp (Oriel), a monochromator (Oriel, $\lambda_{FWHM} = 4$ nm) for selecting the desired wavelength (typically 436 nm), and a photomultiplier (Hamamatsu R928). A two-way amplifier system coupled to the photomultiplier recorded the kinetic response covering the time range from 30 ns to 500 μs and from 1.2 μs to 320 s. Data acquisition of the fast unit was realized by a digital oscilloscope (LeCroy 9310) with a sampling rate of 100 Megasamples per second and a signal resolution of 8 bit. The data of the slower unit were digitized by a 12-bit analog-to-digital converter and averaged in a microprocessor-controlled recorder (home-built) operating on a logarithmic time base. Transient absorption changes could be tracked over 10 decades in time with a dynamic range up to 3.5

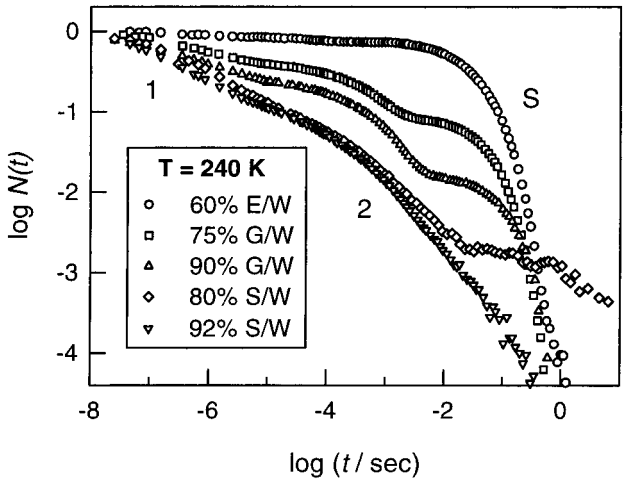

FIGURE 2: Time-dependent survival fraction $N(t)$ of MbCO after photolysis, shown for 60% ethylene glycol/water, 75% and 90% glycerol/water, and 80% and 92% sucrose/water at 240 K on a $\log_{10}$ time scale. The normalization $N(0) = 1$ of the kinetics was determined by using data measured at low temperatures ($T < 140$ K) where rebinding is slow as compared to the experimentally accessible time scale. We applied an initial correction due to temperature-dependent changes of the extinction of MbCO and deoxy-Mb at the monitoring wavelength. Fits to the kinetics were performed with emphasis on the consistency of the total amplitudes for each temperature. This way, we achieved an additional refinement of the normalization. The temperature correction is however below ≈3%.

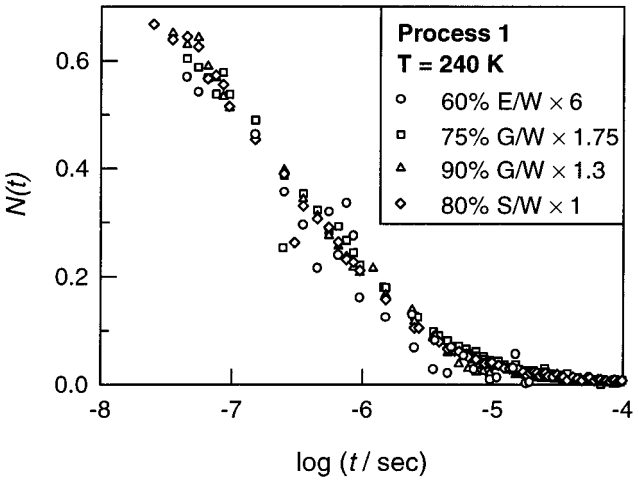

FIGURE 3: Process 1 of CO rebinding to horse myoglobin in four solvents at 240 K. Processes 2 and S have been subtracted, and process 1 of glycerol and ethylene glycol samples is scaled to the amplitude of 80% sucrose/water by factors of 1.3, 1.75, and 6, respectively.

decades in a single shot. The sample was placed in a cell made of two quartz plates that were separated by a 100-μm Teflon spacer. With a myoglobin concentration of 0.6 mM, an optical extinction of ≈1.2 at the Soret peak (424 nm) was reached. The sample cell was mounted in a helium flow cryostat (Air Products) that was regulated by a temperature controller (Lake Shore 330). This setup allowed a temperature accuracy of less than 0.2 K in the desired temperature range from 60 to 300 K.

Depending on the temperature, 15−250 shots were averaged in each measurement. Finally, we obtained a dynamic resolution of approximately 4 decades over a time range of 30 ns to 300 s. In a multiple wavelength study, we observed a small shift of the Soret absorption band on a time scale below 1 μs. The distortion is too small to be relevant at the present level of resolution. We have checked that our kinetic results do not depend on the wavelength within the limits of the given error bars.

RESULTS AND DATA ANALYSIS

Figure 2 shows how the solvent composition at a fixed temperature affects the kinetics $N(t)$ of CO binding to horse skeletal myoglobin. $N(t)$ denotes the survival fraction of molecules that have not rebound their ligand at time t after photolysis. Our measurements resolve three kinetic components, denoted by 1, 2, and S. The rate coefficient of the slowest process S depends on the CO concentration. It represents the bimolecular binding of CO with those myoglobin molecules that have lost the ligand to the solvent after photolysis. Processes 1 and 2 are intramolecular since the corresponding rate coefficients do not vary with the external CO concentration. The cosolvent composition affects mainly the rate and amplitude of process S, decreasing in parallel with increasing solvent viscosity: In 60% E/W about 80% of the photolyzed CO molecules escape to the solvent. In 92% S/W, the escape fraction has dropped to below 10^{-5}, corresponding to a viscosity change by 8 orders in magnitude. This substantial increase has only minor effects on the internal processes 1 and 2. Only the kinetic weight of component 1 appears to increase with the concentration of the cosolvent. A more detailed analysis, involving the subtraction of components 2 and S from $N(t)$, leads to Figure 3, which displays process 1 at 240 K in several solvents. A scale factor has been used to superimpose the kinetic curves as closely as possible. The result of this procedure implies that the characteristic rate and the kinetic shape of component 1 are constant irrespective of the solvent composition. However, the relative magnitude of component 1 depends significantly on the solvent composition as indicated by the scale factors in the insert of Figure 3. Between 60% E/W and 80% S/W, the kinetic weight of process 1 changes by a factor of 6. The effect is too small to be viscosity-related and reflects more likely structural adjustments in response to the cosolvent.

The kinetics of CO binding was studied in five solvents also as a function of the temperature. Figure 4 displays the rebinding kinetics in 80% sucrose/water. The temperature-dependent data set exhibits the same characteristics as those observed in Figure 2 where the cosolvent was varied at fixed temperature. This result suggests a common control parameter, most likely the external viscosity, which can be changed by varying either the temperature or the solvent composition. The bimolecular component S was never observed below the glass temperature of the solvent, which is 227 K for 80% sucrose/water. Figure 4a gives the kinetic curves below T_g, in the glass. At temperatures down to 140 K, one can clearly discriminate two intramolecular components 1 and 2. The relative weight of process 2 decreases however with decreasing temperature. The kinetic curves below 140 K do not show any structure and are thus attributed to process 1. To characterize the kinetic shape of this component requires a rate distribution whose width covers at least 8 orders in magnitude. The same reasoning applies to the 92% S/W sample as shown in Figure 5. The T_g of 92% S/W is close

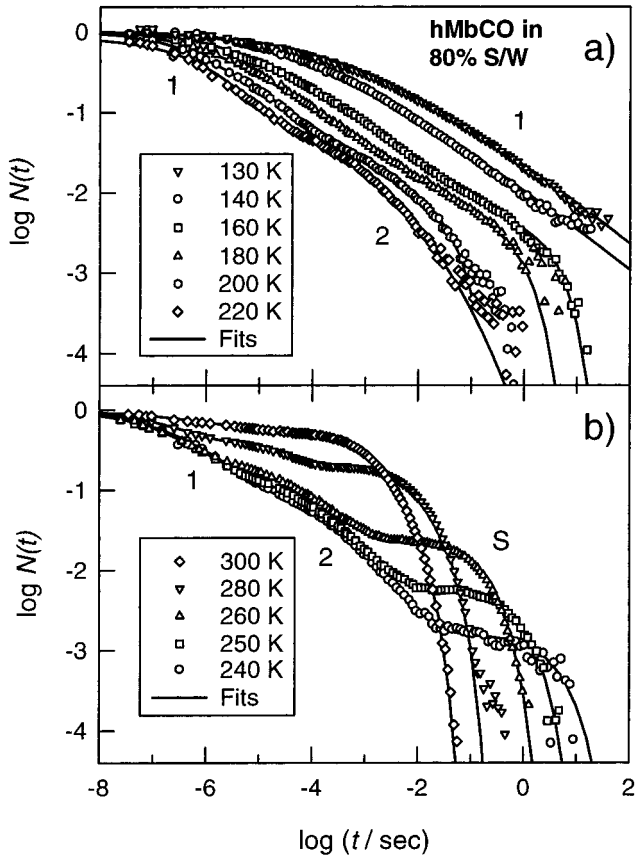

FIGURE 4: Rebinding of CO to horse myoglobin in 80% sucrose/water (a) at low and intermediate temperatures and (b) at high temperatures.

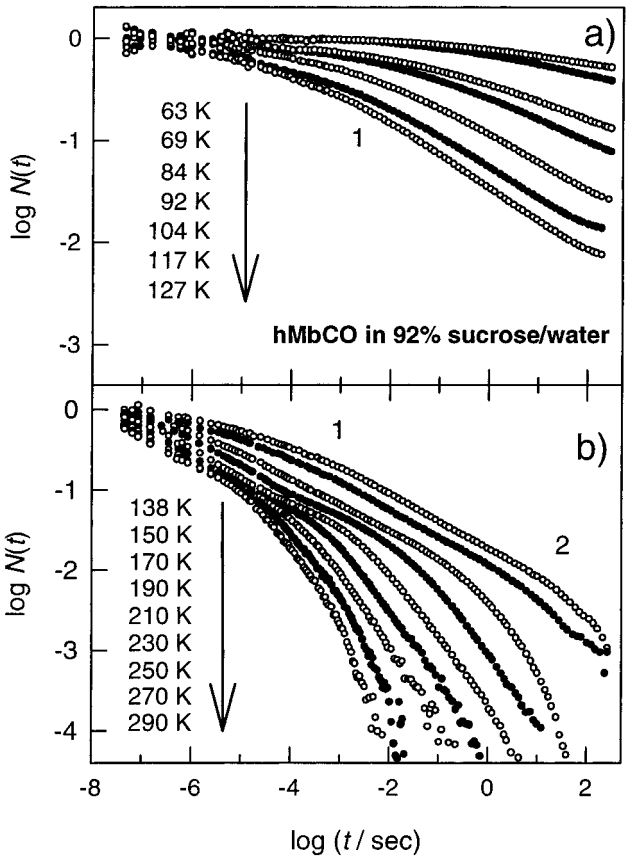

FIGURE 5: Rebinding of CO to horse myoglobin in 92% sucrose/water (a) at low temperatures and (b) at intermediate and high temperatures.

to 280 K. The solvent rebinding process S is thus suppressed as expected for temperatures below T_g.

Viscosity Dependence of the Kinetic Rate Coefficients. The following kinetic analysis is based on eq 3. Details of fit procedures and the calculation of rate coefficients are given in the Appendix. The rate coefficients connecting intramolecular states are viscosity independent and thus change little with the solvent composition. This is shown for k_{CA} in Figure 6a and k_{BC} in Figure 6b. We obtain an average activation enthalpy for C → A of ≈34 kJ/mol. However, for k_{BC} we deduce a systematic solvent composition effect: The numbers determined for the 80% S/W sample are below, and those of the 60% E/W sample are above the values found with the other solvents. These differences are consistent with the reduced amplitude of process 2 relative to process 1 in the 80% sucrose/water sample discussed in the context of Figure 2. The activation energy of B → C amounts to ≈45 kJ/mol depending little on the solvent (Table 2). In spite of this high barrier, k_{BC} exceeds 10^8 s^{-1} at room temperature, which requires a large preexponential $A_{BC} \approx 10^{17}$ s^{-1}. These numbers suggest a complex nature of the inner barrier, which may involve structural changes as well as ligand displacements.

The rate coefficients characterizing the outer barrier in contrast are affected by the bulk solvent viscosity. As discussed above (eq 8), the viscosity is connected with the structural relaxation rate of the solvent. In Figure 7, we display the escape rates k_{CS} in comparison with the solvent relaxation rates $k_S = 1/\tau_S$ determined by specific heat spectroscopy data as shown in Figure 1. The ligand escape

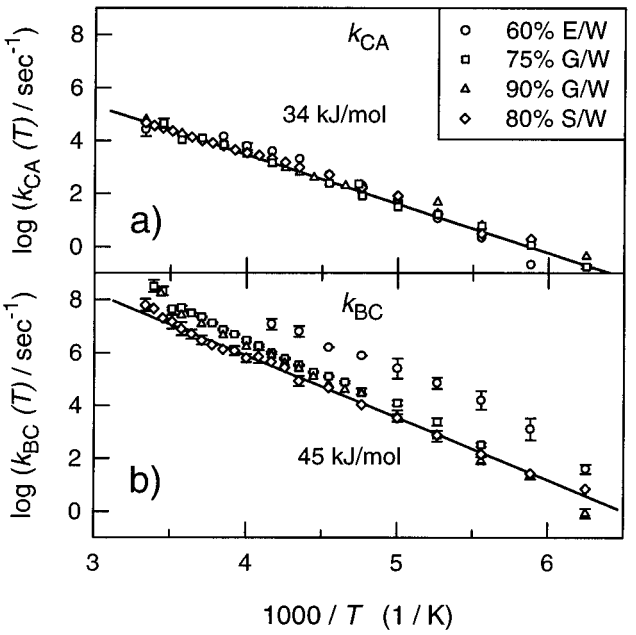

FIGURE 6: Arrhenius plot of protein internal transition rates (a) k_{CA} and (b) k_{BC} for 60% ethylene glycol/water, 75% and 90% glycerol/water, and 80% sucrose/water.

rates are generally much smaller than the structural relaxation times of the solvents. There is only one exception, the corresponding rates of the 80% S/W sample cross at 240 K implying that the bulk solvent structure remains fixed on the time scale of ligand escape below 240 K. The escape rates in general however decrease with increasing solvent

Table 2: Preexponentials A_{BC} and Activation Enthalpies H_{BC} of the Transition B → C, Derived from Arrhenius Fits

solvent	log A_{BC} (s^{-1})	H_{BC} (kJ mol^{-1})
60% E/W	17.5 ± 0.5	47.5 ± 2.5
75% G/W	16.7 ± 0.5	48.3 ± 2.1
90% G/W	16.6 ± 0.4	49.7 ± 2.2
80% S/W	15.3 ± 0.4	44.9 ± 2.1

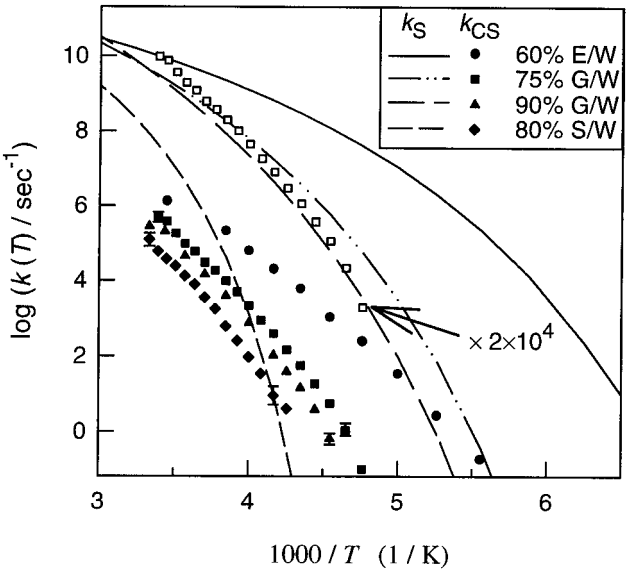

FIGURE 7: Arrhenius plot of ligand escape rates k_{CS} (closed symbols) and solvent relaxation rate k_S (lines) for horse myoglobin in different solvents. For a comparison of the temperature dependence, we additionally show the ligand escape rate of 75% glycerol/water scaled by a factor of 2×10^4 (open squares) to the corresponding solvent relaxation rate.

viscosity. With the exception of 80% sucrose/water, Figure 7 suggests that the escape rate and the bulk relaxation rate exhibit a similar temperature dependence. To show this, we superimpose $k_{CS}(T)$ of 75% G/W with $k_S(T)$ in Figure 7 (open squares). The comparison indicates that the escape rates exhibit a similar but slightly stronger temperature dependence than the bulk viscosity. This observation can be explained by barrier crossing in the high damping limit as described by Kramers law, eq 6. For a quantitative analysis of the viscosity dependence, we use the temperature-dependent viscosity data of Table 1 for each solvent and transform the temperature-dependent ligand escape rates $k_{CS}(T)$ to viscosity-dependent rates $k_{CS}(\eta)$ by eqs 8 and 9. The result is shown in Figure 8. Dashed lines represent fits to the Kramers equation (eq 6), and the solid line gives the $1/\eta$ dependence. Parameters of the fit are summarized in Table 3. We denote the friction-dependent preexponential factor of eq 6 by k_ω/η according to Kramers−Stokes law:

$$k_{CS} = \frac{k_\omega}{\eta} \exp\left(-\frac{H_{CS}}{RT}\right) \qquad (10)$$

The escape rates in 60% ethylene glycol/water, 75% and 90% glycerol/water follow approximately Stokes law, $k_{CS} \propto 1/\eta$. For these solvents, one obtains a solvent-independent barrier characterized by $H_{CS} = 24$ kJ/mol, and a preexponential factor of log k_ω (cP s^{-1}) = 11.5. 80% sucrose/water behaves differently, since the corresponding k_{CS} is less temperature dependent than the bulk viscosity that would require a

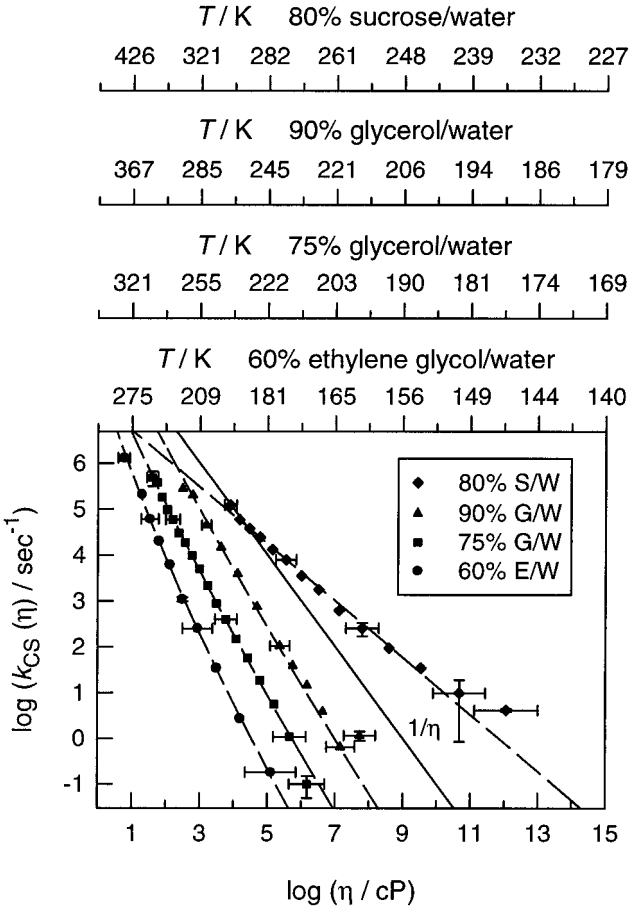

FIGURE 8: Ligand escape rates k_{CS} (symbols) versus solvent viscosity for 60% ethylene glycol/water, 75% and 90% glycerol/water and 80% sucrose/water. Dashed lines represent fits to Kramers−Stokes eq 10 using a fractional viscosity dependence for 90% G/W, and 80% S/W; the solid line shows a $1/\eta$ dependence. On top of the figure for each solvent, the corresponding temperature axis from Figure 7 is shown.

Table 3: Parameters of Fits to Eq 10 for $k_{CS}(\eta)$ Including a Fractional Viscosity Dependence for 80% Sucrose/Water and Values for 90% Glycerol/Water without and with Fractional Viscosity Dependence

solvent	log k_ω (s^{-1} $cP^{-\kappa}$)	H_{CS} (kJ mol^{-1})	κ
60% E/W	11.5 ± 1.2	24.5 ± 5	1
75% G/W	11.5 ± 1.0	23.5 ± 5	1
90% G/W	11.5 ± 1.0	19.5 ± 5	1
90% G/W	11.5 ± 0.3	24.0 ± 3	0.78 ± 0.12
80% S/W	11.0 ± 1.0	25.0 ± 3	0.45 ± 0.05

negative Kramers barrier. A reasonable alternative is to introduce a fractional viscosity exponent κ. Assuming that only the protein−solvent coupling but not the barrier height changes with solvent composition leads to $\kappa = 0.45$ for the escape rates in 80% sucrose/water. The same argument applied to the case of 90% glycerol/water suggests a κ of 0.8 instead of unity. These results indicate that Stokes law may lose its validity at high cosolvent concentration. An equivalent analysis was performed for the reverse transition, k_{SC} (Figure 9). The resulting barrier height comes close to what was found for k_{CS}, suggesting a small enthalpy change upon transfer of the ligand between solvent and the protein matrix (Table 4).

Solvent Effects on Process 1: Activation Energy Spectra. Below 140 K, only component 1 is observed as shown in

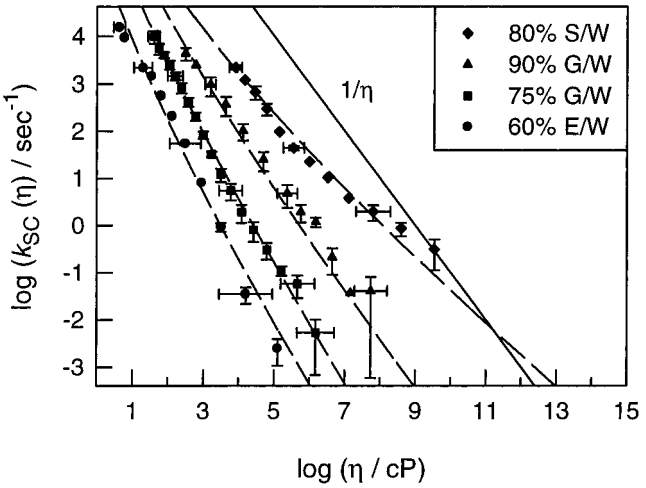

FIGURE 9: Ligand rebinding rates k_{SC} (symbols) versus solvent viscosity for 60% ethylene glycol/water, 75% and 90% glycerol/water, and 80% sucrose/water. Dashed lines represent fits to Kramers−Stokes eq 10 for k_{SC} and H_{SC} using a fractional viscosity dependence for 90% G/W and 80% S/W; the solid line shows a $1/\eta$ dependence.

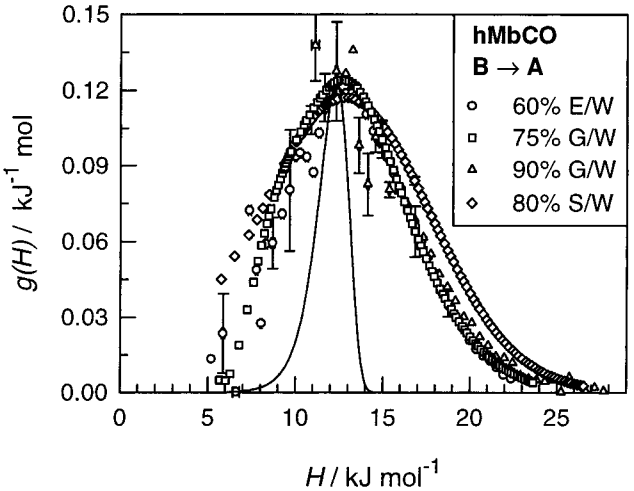

FIGURE 10: Temperature-independent distribution of activation enthalpies $g(H)$ of the internal rebinding step B → A for 60% ethylene glycol/water, 75% and 90% glycerol/water, and 80% sucrose/water. The distributions are calculated by a derivative approximation of the kinetic data. For 60% E/W and 90% G/W, we show curves derived from differentiation of the raw data; for 75% G/W and 80% S/W, we parameterized the kinetics by a polynomial fit before differentiation. The solid line represents the resolution function of the method.

Figures 4a and 5a. The polychromatic kinetic shape of process 1 supposedly reflects the frozen-in structural disorder. Each particular structure of the heterogeneous ensemble contributes an exponential binding curve to the kinetics (Austin et al., 1975; Frauenfelder, 1997). Therefore low-temperature studies can be used to determine solvent effects on structural distributions. Process 1 was analyzed as follows: First we write the survival fraction $N(t)$ as a superposition of exponential terms weighted by a rate distribution $p(k_{BA})$ (Austin et al., 1975; Steinbach et al., 1991; Post et al., 1993):

$$N(t) = \int p(k_{BA}) \exp(-k_{BA}\, t)\, \mathrm{d}k_{BA} \qquad (11)$$

The rate distribution was determined using a derivative approximation (Steinbach et al., 1992). We rewrite eq 11 in the following form, the subscript BA is omitted:

$$-N(t)\frac{\mathrm{d}\log N(t)}{\mathrm{d}\log t} = -t\frac{\mathrm{d}N(t)}{\mathrm{d}t} = -t\frac{\mathrm{d}}{\mathrm{d}t}\int p(k') \exp(-k't)\, \mathrm{d}k' \qquad (12)$$

After performing the derivative and replacing t by $1/k$ and k' and k by $\log k'$ and $\log k$ one obtains:

$$\int p(k')\frac{k'}{k}\exp\left(-\frac{k'}{k}\right)\mathrm{d}k' = \ln 10 \int k'\, g(k')\, 10^{\log k' - \log k} \exp(-10^{\log k' - \log k})\, \mathrm{d}\log k' \qquad (13)$$

The desired function $kp(k)$ appears as a convolution with the resolution function $f(\log k' - \log k)$. Below, we use the approximation $f = \delta(\log k' - \log k)$. This restriction is sufficient for our purpose since $f(\log k' - \log k)$ has a full width at half maximum of 1 decade, but the relevant rate distributions are much broader. To derive the activation enthalpy spectra from temperature-dependent kinetic data, we apply the Arrhenius law:

$$k = k_0 \exp\left(-\frac{H}{RT}\right) \qquad H = RT \ln 10\, (\log k_0 - \log k) \qquad (14)$$

The spectrum of activation enthalpies, assuming the entropy to be sharp (Steinbach, 1996), is then given by

$$g(H) = p(k)\left|\frac{\mathrm{d}k}{\mathrm{d}H}\right| = \frac{kp(k)}{RT} \qquad (15)$$

with the temperature-dependent preexponential (Dlott et al., 1983; Post et al., 1993)

$$k_0 = A\frac{T}{T_0} \qquad T_0 = 100\ \mathrm{K} \qquad (16)$$

Since a different preexponential k_0 leads to a shift of the distribution on the enthalpy axis but not to a change in the shape of $g(H)$ (eq 14), we determined k_0 by fitting the spectra with a parameterized distribution (see Appendix and eq 20) at temperatures below 200 K. These fits resulted in a temperature-independent preexponential factor of $\log A$ (s^{-1}) $= 8.15 \pm 0.15$ for 92% sucrose/water and of $\log A$ (s^{-1}) $= 9.3 \pm 0.15$ for all other solvents. To calculate the derivative in eq 12, we first performed a numerical differentiation of the raw data. Since this was not satisfactory for short times or low enthalpies due to noise, we approximated the kinetics by a least square fit to a polynom on a logarithmic scale. For each data set, $g(H)$ was calculated by polynoms of variable degree ranging from 5 to 15. Direct differentiation of the data and differentiation of the polynom fit led to consistent results shown in Figure 10. The above-mentioned resolution function, transformed to enthalpy space, $f(H, H')$, is also shown. The inverted kinetic data are compatible with temperature-independent activation energy spectra in all solvents examined. Furthermore, the distributions of the different solvents, in spite of large differences in viscosity

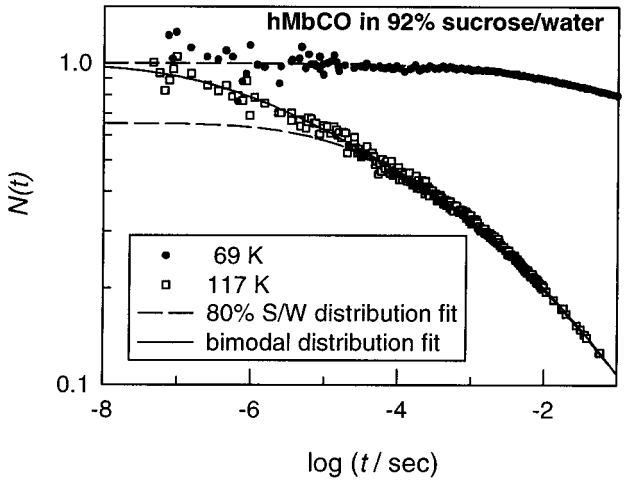

FIGURE 11: Rebinding of CO to horse myoglobin in 92% sucrose/water at 69 and 117 K. The dashed lines represent fits using the enthalpy distribution evaluated for 80% sucrose/water; the solid line is a fit with the bimodal distribution derived for 92% S/W.

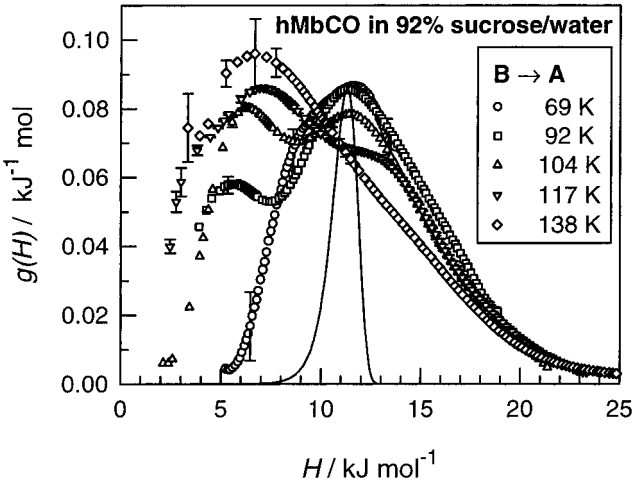

FIGURE 12: Activation enthalpy spectra $g(H)$ of the rebinding step B → A in 92% sucrose/water at low temperatures. The solid line represents the resolution function.

and cosolvent, are nearly identical in shape. However, the high energy tail of the enthalpy distribution broadens consistently with increase in the solvent's glass temperature. The effect is most pronounced for 80% S/W. This suggests that, in solvents with elevated glass temperatures, some high enthalpy conformational states are arrested at T_g that are not populated in solvents near T_g, exhibiting much lower glass temperatures. This effect was predicted by Austin et al. (1975).

Contrasting results were obtained with the 92% S/W sample. Figure 11 displays the CO binding kinetics at 69 and 117 K together with a fit to eq 20 with $g(H)$ for 80% S/W (dashed line). The comparison reveals a fast phase in 92% S/W that is absent at lower cosolvent concentration. Furthermore, the resulting enthalpy distribution shown in Figure 12 exhibits a bimodal shape with maxima near 12.5 and 6 kJ/mol, which strongly depends on the temperature. A fit to eq 20, using a sum of two Gaussian components (eq 21, Appendix), approximates the data even at short times very well (Figure 11, solid line). The structure corresponding to $H_{BA} = 12.5$ kJ/mol, generally found at lower cosolvent concentrations, seems to be more stable at lower temperature. The structure corresponding to $H_{BA} = 6$ kJ/mol may resemble the one found by Hagen et al. (1995) for sperm whale myoglobin in a trehalose glass (6.3 kJ/mol). Our results demonstrate that the structure of myoglobin in the 92% S/W glass can move at temperatures as low as 80 K.

DISCUSSION AND CONCLUSION

Viscosity Effects. The viscosity of glass-forming solvents varies strongly with the temperature. The corresponding activation enthalpies exceed 80 kJ/mol, which is generally much larger than those of protein-related kinetic transitions in water. The use of glass-forming solvents thus allows to select solvent-coupled transitions from intramolecular processes in temperature-dependent experiments at fixed solvent composition. The temperature-dependent structural relaxation times and viscosities of four solvents were derived with the aid of frequency-resolved specific heat experiments. The data displayed in Figures 2 and 3 illustrate that variation of the solvent composition at fixed temperature induces structure-mediated in addition to friction-dependent kinetic effects. The main conclusions based on the analysis of the experimental data according to a directed pathway model can be stated as follows: Intramolecular transitions concerning the kinetic states A, B, and C are insensitive to changes of the bulk viscosity irrespective of the nature of the cosolvent (Figure 6). In contrast, the rate coefficients k_{CS} and k_{SC}, characterizing the ligand transfer across the protein−solvent interface were found to decrease inversely proportional to the bulk viscosity in 60% E/W and 75% and 90% G/W (Figures 8 and 9). The temperature dependence of these rates follows Kramers law of activated escape in the presence of friction, eq 6. For the corresponding Kramers barrier we derive, on the average, 23 ± 5 kJ/mol for C → S and 20 ± 5 kJ/mol for S → C. This property seems to be protein-intrinsic depending weakly on the solvent composition. The enthalpy change of the solvated CO molecule, transfered to a position inside the protein matrix, is therefore small and negative.

The behavior observed with 80% S/W and possibly 90% G/W deviates from this picture since the corresponding rate coefficients exhibit a smaller viscosity dependence than requested by Stokes law. This was accounted for by a fractional viscosity exponent $\kappa < 1$. Best fits are obtained with $\kappa = 0.45$ (80% S/W) and 0.8 (90% G/W), yielding remarkably similar values for the activation enthalpy as obtained for the solvents containing less cosolvent (Table 3). This result suggests that the fractional exponent reflects mainly the solvent composition close to the protein and less likely the shielding of the bulk viscosity by rigid protein structure. The effective viscosity at the protein surface appears to be smaller than in the bulk, which indicates preferential hydration. Timasheff and collaborators (Timasheff, 1993; Lin & Timasheff, 1996) have shown that cosolvent molecules, which stabilize protein structures, are excluded from the protein environment because of an increase in the surface tension. The preferential interaction parameter for sucrose was found to be twice as large as for glycerol (Timasheff, 1993) explaining why 90% G/W shows smaller preferential hydration effects than 80% S/W. Using infrared spectroscopy, we have shown that the O−H stretching frequency of water in the vicinity of the protein is increased as compared to the bulk mixed solvent (Demmel et al., 1997). This result implies softer hydrogen bonds and

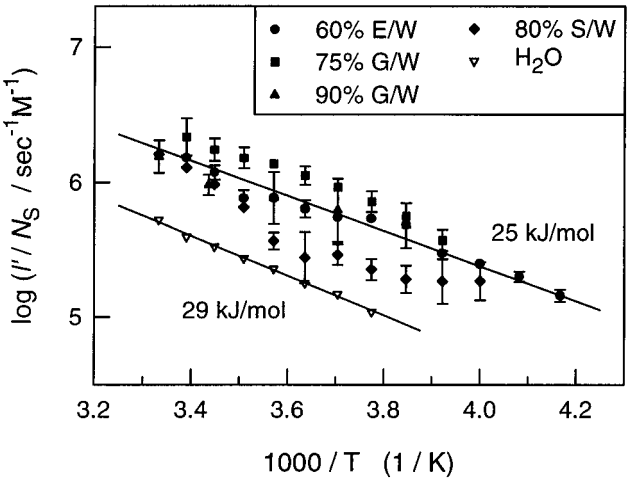

FIGURE 13: Arrhenius plot of the second-order association rate constant of CO, l', normalized by the CO escape fraction N_S in various solvents, 60% ethylene glycol/water, 75% and 90% glycerol/water, 80% sucrose/water, and pure water. The solid lines refer to an activation energy of 25 (upper curve) and 29 kJ/mol, respectively.

less cosolvent in the vicinity of the protein. Mössbauer−Raleigh scattering experiments on proteins in mixed solvents were interpreted in terms of preferential hydration (Goldanskii & Krupyanski, 1995). All fractional viscosity exponents reported in the literature so far did involve kinetic experiments in mixtures (Gavish & Werber, 1979; Gavish, 1980; Beece et al., 1980; Gavish & Yedgar, 1995; Yedgar et al., 1995). It is remarkable that partial demixing and preferential hydration were not considered as a possible explanation of fractional viscosity exponents. Yedgar et al. (1995) at least account for the influence of the cosolvent's molecular weight. Quite analogous results were obtained with hydrated MbCO films as a function of the degree of hydration (Doster et al., 1995). These samples did however contain a small amount of sucrose in order to improve their optical quality. The observed kinetic change thus reflects both the viscosity change in response to reducing the water content and the effect of decreasing hydration.

Solvent Composition Effects. In the preceding sections, we have analyzed the CO recombination kinetics S → A using a sequential two barrier model: The primary barrier, separating the kinetic states S and C, depends on the solvent viscosity while the secondary barrier, controlling C → A, is not affected by dynamical properties of the solvent. Experimentally, we found that both the ligand escape fraction N_S and the pseudo-first-order rebinding rate λ_S of S → A were strongly viscosity dependent. The model predicts, however, that the ratio of λ_S and N_S should be independent of the viscosity. This ratio is given by the product of an intramolecular binding rate, k_{CA}, and the equilibrium coefficient describing the partition of the ligand between solvent and protein matrix (Doster et al., 1982), according to eq 2:

$$\frac{\lambda_S}{N_S} = k_{CA}\frac{k_{SC}}{k_{CS}} \tag{17}$$

To remove also concentration-dependent effects, we multiply the on-rate λ_S by the protein concentration, c_{mb}, which gives the second-order CO association rate constant l' (eq 25, Appendix). Figure 13 plots l'/N_S for water ($N_S \approx 1$) together with results obtained with the mixed solvents ($N_S < 1$).

Table 4: Parameters of Fits to Eq 10 for $k_{SC}(\eta)$ Including a Fractional Viscosity Dependence for 90% Glycerol/Water and 80% Sucrose/Water

solvent	log k_ω (s^{-1} $cP^{-\kappa}$)	H_{SC} (kJ mol^{-1})	κ
60% E/W	8.7 ± 1.2	20.0 ± 5	1
75% G/W	9.0 ± 1.0	20.0 ± 5	1
90% G/W	9.2 ± 0.6	20.0 ± 5	0.8 ± 0.1
80% S/W	8.9 ± 1.9	20.0 ± 5	0.55 ± 0.1

Ideally, if the two-barrier model holds and if solvent composition effects are small, the data points should superimpose. Considering the fact that these solvents can differ in viscosity at a given temperature by several orders in magnitude (Figure 1), the agreement is rather good. However, the l'/N_S in 80% S/W, which is the most viscous solvent, deviates from the linear Arrhenius plot (solid line) at low temperatures. This extreme case, which involves escape fractions below 1%, may indicate the limits of our analysis. Furthermore, the values of l'/N_S obtained in water are systematically below those of the mixed solvents. The difference resides in a smaller preexponential of the Arrhenius law. But the corresponding activation energies of 27 ± 3 kJ/mol (solid lines in Figure 13) for water and the mixed solvents are identical within experimental error. By using eq 2, the values in Figure 6a, Tables 3 and 4 as input, an internal barrier height of 34 kJ/mol together with the negative enthalpy difference of 5 kJ/mol in C relative to S, we obtain 29 kJ/mol in close agreement with the 27 ± 3 kJ/mol, derived above. These results support the existence of solvent-independent enthalpic barriers and represent an important consistency check of our kinetic analysis. The data in Figure 13 also suggest that the addition of cosolvent to an aqueous solution, after correcting for the viscosity change, leads to an increase in the association rate constant of CO with myoglobin. The effect is mainly entropic and may reflect the reorganization of the solvent structure at the protein−solvent interface.

Experiments performed at low temperatures reveal a second intramolecular state B that becomes populated increasingly at the expense of C and S. The B → A and B → C transitions record events close to the heme binding side. A very characteristic feature of process 1 consists of a wide distribution of rebinding rates that narrows with increasing temperature. Numerical inversion of the kinetic curves, assuming the Arrhenius law and enthalpic disorder only, leads to an enthalpy distribution whose shape does not vary significantly with the temperature in the range between 60 and 200 K (Figure 10). Refined global fits of process 1 using a parameterized activation energy distribution (Appendix) revealed a linear temperature drift in the average activation energy. Alternatively, the drift can be attributed to a linear temperature dependence of the prefactor k_0 (eq 16 and below). The latter explanation was adopted because it is in accord with the transition-state theory of simple reactions in condensed phase. It involves a standard entropy S and enthalpy H of activation and predicts the following rate law (Laidler, 1987):

$$k = \frac{k_B T}{h}\exp\left(\frac{S}{R}\right)\exp\left(-\frac{H}{RT}\right) \tag{18}$$

The change in the effective activation energy due to the

temperature-dependent prefactor between 60 and 200 K is less than 2 kJ/mol. This effect was detected only because of the relatively small activation enthalpy in the spectral range between 5 and 10 kJ/mol (Figure 10) and precise measurements covering a wide temperature range. The kinetic transitions involving the states C and S are controlled by much larger enthalpies, and the correction then becomes insignificant. We thus assume all prefactors except k_0 to be constant (Appendix). The linear temperature dependence of k_0 was noticed before with horse (Post et al., 1993) and sperm whale myoglobin (Austin et al., 1975; Srajer et al., 1988; Steinbach et al., 1991).

As Figure 10 shows, the enthalpy spectrum changes very little with the solvent composition; the peak enthalpy is always close to 13.4 ± 0.5 kJ/mol. The enthalpy spectrum presumably reflects the distribution of structural states frozen-in at the glass temperature of the solvent (Austin et al., 1975; Frauenfelder et al., 1979; Parak et al., 1982; Iben et al., 1989), implying that the average structure of the protein changes little with temperature and solvent composition. The 92% S/W sample however shows very surprising rebinding kinetics below 140 K (Figure 11). The corresponding enthalpy distribution, $g(H)$, in contrast to what has been said above, has a bimodal shape and varies with the temperature (Figure 12). The distribution peaks near 12.5 kJ/mol below 100 K as expected, but a shoulder near 5−6 kJ/mol is emerging at higher temperatures. Hagen et al. (1995) have observed a similar low peak enthalpy of 6.3 kJ/mol in their experiments of swMb embedded in a trehalose glass. Their measurements were restricted to temperatures above 100 K. These authors therefore did not observe the particular shape and temperature dependence of $g(H)$ that becomes evident only below 100 K. But even above 100 K, they found it difficult to fit the data using a temperature invariant enthalpy spectrum. To keep the enthalpy spectrum temperature independent, Hagen et al. (1996) introduce a distributed prefactor. Although a unique solution defining the enthalpy and entropy distribution cannot be obtained based on kinetic data alone, a temperature-dependent $g(H)$ seems more natural for the following reason. It is well known for sperm whale myoglobin that at least three taxonomic substates A_0, A_1, and A_3 contribute to $g(H)$ that are classified according to the stretching frequency of bound CO (Johnson et al., 1996). A_1 represents the majority state under physiological conditions, while A_0 dominates at low pH or low hydration (Ansari et al., 1987; Brown et al., 1983). Furthermore, the relative weight of A_0 increases continuously with decreasing temperature in hydrated myoglobin (Mayer, 1994). A crystallographic study has shown that the imidazole side chain of His64, which is interacting with the ligand in states A_1 and A_3, has moved out of the heme pocket in substate A_0 (Yang & Phillips, 1996). The kinetics of individual substates, monitoring their C−O stretching bands, led to the following peak enthalpies of B → A: A_0, 8 kJ/mol; A_2, 10 kJ/mol; A_3, 19.5 kJ/mol (Johnson et al., 1996). Using comparable peak values and A-state populations, we could construct the $g(H)$ for horse myoglobin in 75% G/W consistent with the kinetic data (Post, 1994). These results and $g(H)$ in Figure 12 suggest that hMbCO in 92% sucrose/water mainly populates A_0 above 130 K, but reverts to A_1 at lower temperatures. The fraction of state A_3 remains constant. The imidazole of His64 is supposed to become deprotonated and rotate back into the heme pocket at temperatures as low as 80 K. Similar observations, that the conformers in hydrated MbCO interconvert over the whole temperature range down to 78 K, were reported by Mayer (1994). The data in Figure 12 apparently display the A_0/A_1 exchange. No time-dependent shifts were noticed on a time scale of hours, suggesting that the equilibrium has been reached. It follows that A_1 of hMbCO in 92% S/W represents the ground state because of its low enthalpy. The larger entropy favors state A_0 at higher temperatures. For a quantitative analysis, we performed fits to the distribution $g(H)$ using a sum of three Gaussians corresponding to three populations (eq 21, Appendix). The fitting routine we applied to the data was based on a Marquardt−Levenberg algorithm (Press et al., 1986) and specified constraints for keeping peak positions and distribution widths within a reasonable range. The resulting temperature dependence of each population is shown in Figure 14. The opposite temperature dependence was found in aqueous solutions, suggesting that A_0 is energetically stabilized, while the conformer A_1 dominates at neutral pH because of its larger entropy (Ansari et al., 1987). Furthermore the exchange between the substates is arrested at the freezing or glass temperature of the solvent. Our results indicate some residual protein mobility in the glass at high cosolvent concentration, possibly as a result of mobile water pockets and preferential hydration.

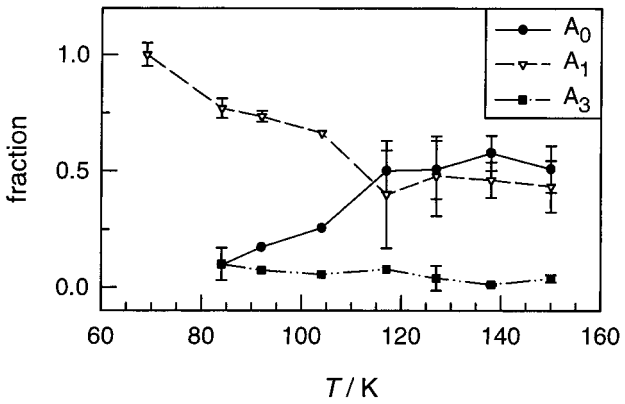

FIGURE 14: Temperature dependence of the substate populations A_0, A_1, and A_3, derived from $g(H)$ for 92% sucrose/water. The lines are shown to guide the eyes.

Apart from this extreme situation at 92% by weight cosolvent content, process 1 shows little change in its time dependence with solvent composition. However, above 200 K, where processes 2 and S become noticeable, we find that the kinetic fraction of process 1 increases continuously, most likely in response to larger cosolvent concentrations. It follows that k_{BC} has to decrease in parallel, by a factor of 6 if 60% E/W and 80% S/W are compared (Figure 6b). The question of how the transition from B to C can be modified is of considerable importance, since intermediate C supposedly controls the rebinding under physiological conditions (Steinbach et al., 1991; Tian et al., 1992; Post et al., 1993; Agmon et al., 1994). While the bound state A, the geminate pair state B, and the deoxy state S of myoglobin are structurally well characterized (Kuriyan et al., 1986; Schlichting et al., 1994; Hartmann et al., 1996; Srajer et al., 1996; Takano, 1977), little is known about the C intermediate: Two well-separated processes 2 and 3 are observed with swMbCO while only a single process is sufficient to explain the oxygen

binding kinetics (Steinbach et al., 1991). With horse myoglobin, as shown above, a single, but slightly nonexponential process accounts for the CO binding kinetics (Post el al., 1993). However, we recently found, using periodic photolysis, that process 2, as in the case of swMb, is separable into two kinetic components, 2 and 3 (unpublished experiments). The difference between the CO and O_2 recombination kinetics points to a ligand-specific C intermediate. Possibly, the dipole of the CO molecule in state C interacting with HisE7 assumes two energetically nonequivalent states, which are degenerate in the case of the symmetric dioxygen molecule.

Energy Landscape and Kinetic Scheme. An important question is whether the kinetic constants of CO binding to myoglobin obtained at low and intermediate temperatures with mixed solvents can be extrapolated to physiological conditions. Such a low temperature analysis of swMbCO in 75% G/W, using a sequential kinetic scheme of four states (A, B, C, S) predicts that the B → A transition will limit the overall CO rebinding rate at room temperature (Doster et al., 1982). This result is incompatible with experimental evidence for the following reasons: The recombination kinetics of MbCO in water at 300 K allows us to discern only two kinetic components (Henry et al., 1983). The slow phase can be assigned to CO binding from the solvent, denoted by S; the fast component involves intramolecular binding and ligand escape across the protein−solvent interface. The two-component kinetics implies only three effective states. We thus go back to the scheme of eq 1 and ask whether B or C represent the relevant intramolecular state. Experimentally one observes for both, swMbCO (Henry et al., 1983) and hMbCO, that the photodissociated CO molecule escapes to the solvent with probability $N_S \approx 0.96$ at 300 K. Furthermore, we obtain for the rate of the fast component of hMbCO, $\lambda_1 = 5.8 \times 10^6\ s^{-1}$, which is similar to what was found for swMbCO (Henry et al., 1983). According to eq 1, λ_1 is given by the sum of an intramolecular binding rate and the ligand escape rate

$$\lambda_1 = k_{(B)CA} + k_{(B)CS} \qquad (19)$$

depending on whether the relevant intramolecular state is B or C. Since 96% of all photolyzed ligands escape to the solvent, it follows from eq 2 that $\lambda_1 \approx k_{(B)CS}$. By extrapolating the low temperature results to 300 K, we obtain for the averaged $k_{BA} = 8 \times 10^6\ s^{-1}$. According to eq 2, this value gives an escape fraction of 0.42, quite different from the experimental value of 0.96. From the experimental escape fraction, we calculate (eq 2) a geminate rate coefficient near $10^5\ s^{-1}$. Figure 6a demonstrates that k_{CA} and not k_{BA} have approximately the correct value at 300 K. This shows that states C and not B qualifies as the relevant final step of rebinding from the solvent.

To reconcile these results with experiments performed within a wide temperature and viscosity range, we introduced the directed pathway model of eq 3, which includes the relaxation step B → C. Figure 15 shows a sketch of the resulting free energy landscape at 300 K. The conformational coordinate can be given only in arbitrary units, but the energy axis reflects the quantitative kinetic analysis with respect to the following conditions. Position B serves as the reference state. The outer barrier has been adjusted to 1 cP; the viscosity of water was at 20 °C. It was assumed that structural relaxation, B → C, lowers the free energy of the protein−ligand system, leading to state C, but does not affect the height of the saddle points. Such an assumption is required since the structural change dissipates the information about the energy difference between B and C. The standard free energy G and entropy S of activation were determined using the rate law of eq 18 and the data given in the Tables 2−4, with $k_B T/h = 10^{13}\ s^{-1}$ at 300 K: $G = H - TS$. Figure 15 visualizes why most of the ligands escape to the solvent from B and why the C → A transition is rate limiting to both intra- and extramolecular binding at room temperature. Figure 16a,b displays projections of the free energy and the enthalpy surfaces for both directions, 'in' and 'out', corrected to a viscosity of 1 cP. As the reference state either B (out) or S (in) was chosen. This plot allows us to assess the influence of solvent composition on ligand escape and rebinding. Corrected for the viscosity, the barriers prove to be remarkably resistant to changes in the solvent composition. This applies to the free energy and enthalpy diagrams of both directions, "in" and "out". The important exception consists in the free energy barrier controlling the relaxation step, B → C, which increases significantly at high cosolvent concentration. The difference explains the enhanced rebinding from B at low water content, discussed in the context of Figure 3. Since the corresponding activation enthalpy is constant, one has to assign the solvent effect to entropic differences. A related observation was reported by Sage et al. (1995). The heme-coupled structural relaxation monitored by the Fe−His frequency slows down if glycerol is added to an aqueous solution. The study also shows that glycerol perturbs the equilibrium structure of the protein.

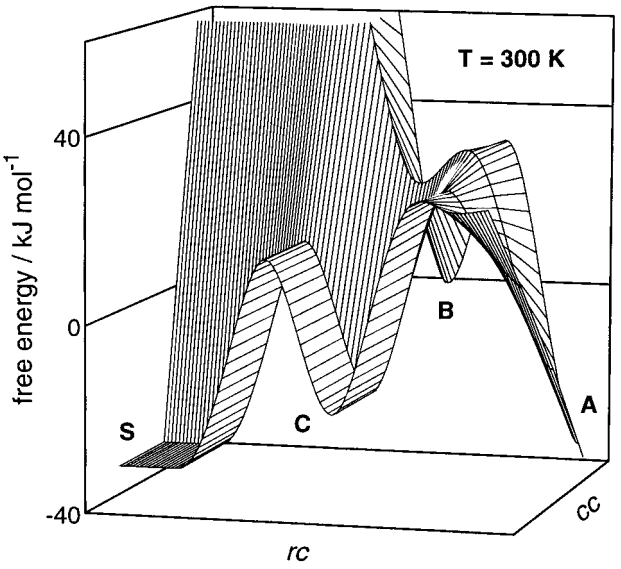

FIGURE 15: Free energy surface as a function of the reaction coordinate *rc* and the conformation coordinate *cc*. The values for the different barriers are derived from hMbCO in 75% glycerol/water at 300 K. The external barrier separating C and S is corrected to a viscosity of 1 cP. B was chosen as the reference state.

The free energy diagram of 60% E/W in Figure 16a approximates the situation in pure water. At high temperatures, more than 99% of all molecules go from B to C within a few nanoseconds. From C, 96% escape to S within 200 ns. Rebinding from C to A would take about 10 μs. The

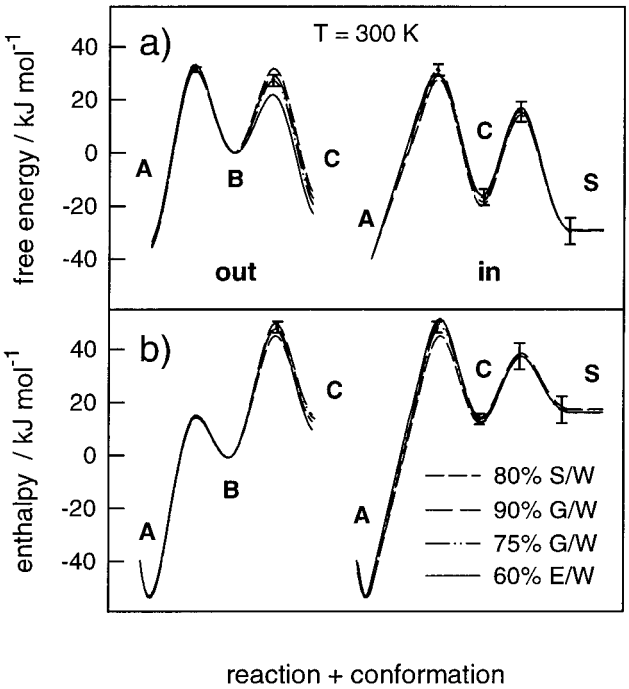

FIGURE 16: Projections of the energy surface shown in Figure 15 displaying (a) the free energy calculated at 300 K and (b) the enthalpy, for 60% ethylene glycol/water, 75% and 90% glycerol/water, and 80% sucrose/water. 'out' refers to the projection A−B−C, 'in' refers to the projection S−C−A.

overall rebinding from S follows eq 1, a fast preequilibrium between S and C in sequence with the terminal step C → A. The free energy difference between S and C appears to be mainly entropic. It is likely to reflect the loss of translational entropy of the ligand entering the heme pocket.

Srajer et al. (1996) monitored the dynamics of the MbCO complex at room temperature using nanosecond time-resolved crystallography. In their time-resolved X-ray study of swMbCO, they report that the plausible docking site of photolyzed CO is still occupied after 4 ns. The corresponding electron density difference has disappeared at 1 μs. The authors attribute this feature tentatively to ligand escape to the protein surface. This interpretation leads to a surprisingly large second-order association rate, $l' = 2.5 \times 10^6$ s^{-1}, five times larger than in solution. However, the two component kinetic data, presented in their Figure 2, nearly coincide with processes 1 and 2, observed in high viscosity solvents (Figures 2 and 4b). This alternatively suggests that states C and not S may be populated after 1 μs, implying an intramolecular ligand displacement to a less well defined position. The loss of electron density in the photolyzed state was reported even for the initial docking site visible at 4 ns, which accounts for only 40% of the photolyzed CO molecules.

Nature of Intermediate C: Blocking Water Hypothesis. Since the number and the properties of the C and D intermediates depend on the nature of the ligand (Steinbach et al., 1991), it is suggestive that the B → C transition involves a displacement of the ligand. The CO molecule may reorient or move to a slightly different position. The CO stretching frequency does not change significantly, excluding a major displacement (Nienhans et al., 1994). It is thus difficult to envision how such a minor shift could decrease the rebinding rate by 3 orders in magnitude. Apart from invoking structural adjustments on the proximal side and relaxation of the heme group, there is another interesting possibility that involves the distal side of the heme: The heme pocket of deoxy-myoglobin contains a non-coordinated water molecule, hydrogen-bonded to His64. This molecule is no longer present in the CO-bound structure (Kuriyan et al., 1986; Quillin et al., 1995), although a weakly occupied water site in the heme pocket was suggested for oxy-myoglobin (Phillips, 1980). This raises the question of whether the removal of the distal pocket water by the ligand plays a role in the formation of intermediate C. We have shown that the decay of the C intermediate, together with a fast preequilibrium between S and C, determines the overall rebinding of CO from the solvent under physiological conditions (eq 1). This leads to the following question: Does the removal of the distal water molecule by CO upon binding take place in step with the fast preequilibrum C ⇌ S or does it limit the access to the heme binding site contributing to the C → A barrier?

Our experiments show that state C becomes populated after photolysis at temperatures as low as 140 K (Figures 4a and 5). In this range the solvent is frozen, implying that the photolyzed ligand remains confined to the heme pocket. Thus, assuming that a water molecule contributes to the formation of state C, it has to be intramolecular. It is a striking fact that water molecules in a heterogeneous environment, such as amorphous ice, start to become mobile in the temperature range near 140 K (Johari et al., 1987; Hallbrucker et al., 1989; Sartor et al., 1994). Such a peripheral water may occupy the B binding site after the ligand has moved to a new position C.

The distal pocket of aquo-metmyoglobin contains an additional well defined water molecule that is supposed to be hydrogen-bonded to the water molecule coordinated to the heme iron (Quillin et al., 1993, 1995). This shows that, in addition to the ligand, there is enough space available for a water molecule in the heme pocket. Interestingly, no corresponding discrete electron density peaks were found in the structures of distal pocket metmyoglobin mutants (Quillin et al., 1995). Kinetic experiments and crystallographic and spectroscopic studies by Cameron et al. (1993) and Quillin et al. (1995) on myoglobin mutants, where the distal His64 was replaced by aliphatic side chains, have revealed an inverse correlation between the stability of the non-coordinated water and the CO association rate constants: The loss of polarity in the heme pocket accelerates the binding kinetics (Li et al., 1994). These authors conclude that it is the hydrogen bond interaction to His64 that inhibits ligand binding, since the non-coordinated water molecule has to be displaced before the iron becomes accessible to the ligand (Cameron et al., 1993). The displacement of the distal pocket water supposedly constitutes the major equilibrium and kinetic barrier to ligand binding (Carver et al., 1990; Rohlfs et al., 1990). Quillin et al. (1995) analyzed their room temperature kinetic data using a three-well model with kinetic states A, C, and S in our notation. This allows the discussion of the control of ligand binding in terms of an outer barrier S → C followed by an inner kinetic barrier of C → A. The removal of the pocket water presumably contributes to both kinetic barriers. In contrast, previous structural interpretations predicted that the salt bridge formed by Arg45 and the heme-6-propionate side chain would control the access to

the heme pocket (Ringe et al., 1984; Perutz, 1989). However rather drastic substitutions at position 45 or elimination of the salt bridge using protoheme IX dimethyl ester-substituted myoglobin produced little effect on the association rates of O_2, CO, and NO but increased the rates of larger isocyanide ligands (Carver et al., 1991). A nuclear magnetic resonance and kinetic study on a triple mutant also found no significant effects of the side chain at position 45 on the ligand kinetics (Travaglini Allocatelli et al., 1993). These results suggest either alternative pathways for small ligands or a high structural flexibility of this solvent-exposed area, which is stretched to its limits by large ligands. The CO association kinetics of native myoglobin at physiological temperature and low viscosity is controlled by the inner barrier height C → A relative to the free energy in state S and not by the outer barrier (Doster et al., 1982). However, the situation can be reversed by increasing the viscosity that allows the study of the anatomy of the outer barrier. Apart from an inverse solvent viscosity dependence of the prefactor, we consistently derive an activation enthalpy of 20 kJ/mol in several solvents for the outer barrier and a stabilization by 5 kJ/mol in C relative to S. An interpretation consistent with the mutant studies would assign the enthalpy to breaking of the hydrogen bond of the distal water molecule with His64, which is intramolecular. The viscosity dependent prefactor could reflect the dynamics of the gate formed by Lys45, which replaces the arginine at position 45 in horse myoglobin, and the propionate side chain.

In studies of mutant swMb, replacing His64 by less polar side chains uniformly lowers both kinetic barriers irrespective of their size (Carver et al., 1990; Smerdon et al., 1991). This result is consistent with the interpretation that destabilization of the pocket water by apolar substitution of His64 reduces the outer barrier but suggests further effects on the inner kinetic barrier. Lambright et al. (1993) have performed kinetic experiments on distal pocket mutated sperm whale myoglobin at lower temperatures and could resolve up to four kinetic components. They report that the C → S transition is not affected by distal pocket mutations in contrast to S → C. However, the geminate rates are generally enhanced by nonpolar mutations. For instance, in the His64 to Ala mutant, process 1 appears to be similar to the wild type kinetics. However the amplitude of processes 2 and S are reduced significantly. This result implies that the formation of intermediate C is suppressed because of a lower B → C transition rate. A plausible interpretation of this result and those mentioned above could be that the formation of intermediate C out of B involves the interaction with an intramolecular water molecule that is close to or inside the pocket. Our experiments indicate that osmotic stress imposed by increasing the cosolvent concentration also reduces k_{BC} without affecting k_{BA} (Figures 3 and 6b) since the relative weight of component 1 but not its time dependence is changing with the cosolvent composition. Our hypothesis implies that the occupation of the intramolecular water site decreases with the external water activity. Cameron et al. (1993) have suggested, based on the work of Brown et al. (1983), that increasing hydration favors the protonation of the N_ϵ and deprotonation of N_δ of His64. Furthermore, process 2 is observed at temperatures as low as 138 K even in solvents that are glassy at room temperature (Figure 5b; Hagen et al., 1996). This behavior is consistent with a transition requiring small diffusive motions of, for instance, a peripheral water molecule in the heme pocket.

The CO binding kinetics of horseradish peroxidase (HRP) in contrast is deficient of a C intermediate. The geminate phase above 200 K consists of process 1, which is much faster than for MbCO (Doster et al., 1987). The speed of bimolecular rebinding, S → A, however, is by a factor of almost 1000 lower than for MbCO. A high outer barrier of 50 kJ/mol dominates rebinding opposite to MbCO, where the inner barrier is more important (Doster et al., 1982). The absence of intermediate C would suggest, according to our hypothesis, that the heme pocket of HRP excludes water more strongly than does myoglobin. Intermediate C thus accelerates both escape and bimolecular binding by facilitating the access of hydrated ligands to the heme pocket.

Conclusion. Our kinetic study of CO binding to horse myoglobin in several mixed solvents allows us to separate solvent composition from viscosity-related effects. Only the outer barrier depends on the bulk viscosity, but at high cosolvent concentration partial demixing and preferential hydration lead to an apparently reduced viscosity effect. Analysis according to Kramers law of activated escape in the presence of friction reveals a protein-intrinsic outer barrier of 20−25 kJ/mol, depending little on the solvent composition. A small but significant solvent dependence was noticed for the intramolecular transition B → C. Increasing the osmotic stress by large cosolvent concentrations decreases the population of intermediate C. We therefore suggest that a water molecule contributes to the formation of state C. The B → C transition apparently involves a structural change since the derived energy landscape cannot be reconciled with a simple kinetic mechanism. It follows that intermediate C and not intermediate B controls the bimolecular rebinding rate. But, in contrast to intermediate B, little structural information of intermediate C is available. We have emphasized the possible role of structural changes on the distal side involving His64 and possibly a water molecule. Further investigations aiming to uncover the nature of intermediate C will provide important missing details on the mechanism of ligand binding. The free energy landscape of Figure 15 suggests that thermal dissociation of bound CO may also bypass the B intermediate.

ACKNOWLEDGMENT

We are grateful to Dr. F. Post and D. Müller for technical support and to M. Hernler for participation in the 92% sucrose/water sample measurements.

APPENDIX: FITTING PROCEDURES AND PROTEIN TRANSITION RATES

Fitting Procedures. We used three functions to fit the recombination processes 1, 2, and S. Process 1 was analyzed in terms of an enthalpy distribution $g(H_{BA})$:

$$N_1(t) = N_1 \int g(H_{BA}) \exp(-k(H_{BA})t)\, dH_{BA} \quad (20)$$

where H_{BA} and $g(H_{BA})$ are related to $k(H_{BA})$ and $p(k)$ by eqs 14 and 15. To derive the enthalpy distribution $g(H_{BA})$, we utilized three methods. First, we performed a fit of eq 20 to the kinetics assuming an analytical form, the Gamma function for $g(H_{BA})$ (Young & Bowne, 1984). Second,

$g(H_{BA})$ was obtained by kinetic inversion using the derivative approximation (Steinbach et al., 1992). Finally, the enthalpy distribution was approximated by a sum of three Gaussian distributions representing the population of three conformational substates, A_0, A_1, and A_3, known from infrared work (Ansari et al., 1987):

$$g(H_{BA}) = \sum_i \frac{n_i}{\sqrt{2\pi}\sigma_i} \exp\left(-\frac{(H_{BA} - H_p^{(i)})^2}{2\sigma_i^2}\right) \quad (21)$$

with

$$\sum_i n_i = 1 \qquad i = 0, 1, 3$$

n_i gives the relative fraction of each substate A_i, $H_p^{(i)}$ is the correspondent peak enthalpy, and σ_i is the width parameter. Process 2 was approximated by a Kohlrausch−Williams−Watts (KWW) function (Williams & Watts, 1970):

$$N_2(t) = N_2 \exp\left(-\left(\frac{t}{\tau}\right)^{\beta}\right) \quad (22)$$

The characteristic rate coefficient of a KWW function follows from the average decay time (Lindsey & Patterson, 1980):

$$1/\lambda_2 = \langle\tau\rangle = \frac{\tau}{\beta}\Gamma\left(\frac{1}{\beta}\right) \quad (23)$$

where $\Gamma(x)$ is the Gamma function. The bimolecular process S was analyzed by the differential equation for the concentration of ligated protein c_{mbco}

$$\frac{dc_{mbco}}{dt} = l'(c_{co} - c_{mbco})(c_{mb} - c_{mbco}) \quad (24)$$

where c_{mb} denotes the total concentration of myoglobin and c_{co} refers to the total concentration of CO. Solving eq 24 yields the time-dependent fraction of unligated myoglobin for process S:

$$N_S(t) = N_S\left(1 - \frac{c_{mbco}(t)}{c_{mb}}\right) = N_S \frac{\upsilon - 1}{\upsilon \exp[(\upsilon - 1)\lambda_S t] - 1} \quad (25)$$

with

$$\upsilon = \frac{c_{co}}{c_{mb}}$$

λ_S has the dimension of a pseudo-first-order rate and is given by the ratio of the second-order rate l' and the total protein concentration c_{mb}. The normalized amplitudes, N_1, N_2, and N_S, display the relative fraction of each rebinding process.

Transition Rate Calculation. In the model of eq 3, the average of the rate coefficient k_{BC} is determined in a self-consistent procedure accounting for the nonexponential shape of process 1 in terms of $g(H_{BA})$:

$$N_2 = \int g(H_{BA}) \frac{k_{BC}}{k(H_{BA}) + k_{BC}} dH_{BA} \quad (26)$$

The integral is then calculated self-consistently by varying k_{BC} until it comes close to the experimentally determined N_2. The rate coefficients k_{CA}, k_{CS}, and k_{SC} were derived based on the scheme of eq 3, which implies the following set of differential equations:

$$\dot{\mathbf{N}}(t) = \mathbf{K}\mathbf{N}(t) \quad (27)$$

where $\boldsymbol{N}(t)$ denotes the population vector whose components $N_i(t)$ describe the occupation of the four states, A, B, C, and S; and $\mathbf{K}$ refers to the transition matrix, containing the rate coefficients k_{ij}:

$$\mathbf{N}(t) = \begin{pmatrix} N_A(t) \\ N_B(t) \\ N_C(t) \\ N_S(t) \end{pmatrix}$$

$$\mathbf{K} = \begin{vmatrix} 0 & k_{BA} & k_{CA} & 0 \\ 0 & -k_{BA} - k_{BC} & 0 & 0 \\ 0 & k_{BC} & -k_{CA} - k_{CS} & k_{SC} \\ 0 & 0 & k_{CS} & -k_{SC} \end{vmatrix} \quad (28)$$

The flash photolysis experiment yields $N(t) = 1 - N_A(t)$. The fits to the kinetics allow to determine the recombination rate coefficients λ_1, λ_2, and λ_S, which are the eigenvalues of the transition rate matrix $\mathbf{K}$. Due to the small off-rate of MbCO, we exclude thermal dissociation on the time scale of our experiment, and thus, the dissociation rate k_{AB} is assumed to vanish. This allows to eliminate the fourth eigenvalue. Since process S is always much slower than intramolecular binding, we further assume k_{SC} to be small as compared to the other rate coefficients. With these approximations, we evaluate after some algebra the rate coefficients from the eigenvalues of the matrix $\mathbf{K}$ and the amplitudes of the recombination processes:

$$k_{CA} = \lambda_2 \frac{N_2}{N_2 + N_S}$$

$$k_{CS} = \lambda_2 \frac{N_S}{N_2 + N_S} \quad (29)$$

$$k_{SC} = \lambda_S \frac{N_2 + N_S}{N_2}$$

The enthalpy of each transition $i \rightarrow j$ was determined using a fit of the Arrhenius equation to the temperature-dependent transition rates:

$$k_{ij} = A_{ij} \exp\left(-\frac{H_{ij}}{RT}\right) \quad (30)$$

where A_{ij} is the preexponential factor.

REFERENCES

Agmon, N., & Hopfield, J. J. (1983) *J. Chem. Phys. 79*, 2042−2053.
Agmon, N., & Sastry, G. M. (1996) *Chem. Phys. 212*, 207−219.
Agmon, N., Doster, W., & Post, F. (1994) *Biophys. J. 66*, 1612−1622.
Ansari, A., Berendzen, J., Braunstein, D., Cowen, B. R., Frauenfelder, H., Hong, M. K., Iben, I. E. T., Johnson, J. B., Ormos,

P., Sauke, T. B., Scholl, R., Schulte, A., Steinbach, P. J., Vittitow, J., & Young, R. D. (1987) *Biophys. Chem. 26*, 337−355.
Ansari, A., Jones, C. M., Henry, E. R., Hofrichter, J., & Eaton, W. A. (1992) *Science 256*, 1796−1798.
Ansari, A., Jones, C. M., Henry, E. R., Hofrichter, J., & Eaton, W. A. (1994) *Biochemistry 33*, 5128−5145.
Austin, R. H., Beeson, K. W., Eisenstein, L., Frauenfelder, H., & Gunsalus, I. C. (1975) *Biochemistry 14*, 5355−5373.
Beece, D., Eisenstein, L., Frauenfelder, H., Good, D., Marden, M. C., Reinisch, L., Reynolds, A. H., Sorensen, L. B., & Yue, K. T. (1980) *Biochemistry 19*, 5147−5157.
Beece, D., Bowne, S. F., Czege, J., Eisenstein, L., Frauenfelder, H., Good, D., Marden, M. C., Marque, J., Ormos, P., Reinisch, L., & Yue, K. T. (1981) *Photochem. Photobiol. 33*, 517−522.
Birge, N. O. (1986) *Phys. Rev. B 34*, 1631−1642.
Birge, N. O., & Nagel, S. R. (1985) *Phys. Rev. Lett. 25*, 2674−2676.
Brown, W., III, Sutcliffe, J. W., & Pulsinelli, P. D. (1983) *Biochemistry 22*, 2914−2923.
Bulone, D., Donato, I. D., Palma-Vitorelli, M. B., & Palma, M. U. (1991) *J. Chem. Phys. 94*, 6816−6826.
Cameron, A. D., Smerdon, S. J., Wilkinson, A. J., Habash, J., Helliwell, J. R., Li, T., & Olson, J. S. (1993) *Biochemistry 32*, 13061−13070.
Carver, T. E., Rohlfs, R. J., Olson, J. S., Gibson, Q. H., Blackmore, R. S., Springer, B. A., & Sligar, S. G. (1990) *J. Biol. Chem. 265*, 20007−20020.
Carver, T. E., Olson, J. S., Smerdon, S. J., Krzywda, S., Wilkinson, A. J., Gibson, Q. H., Blackmore, R. S., Ropp, J. D., & Sligar, S. G. (1991) *Biochemistry 30*, 13061−13069.
Colombo, M. F., Rau, D. C., & Parsegian, V. A. (1992) *Science 256*, 655−659.
Crowe, L. M., Reid, D. S., & Crowe, J. H. (1996) *Biophys. J. 71*, 2087−2093.
Cupane, A., Vitrano, E., & Cordone, L. (1986) *J. Mol. Biol. 189*, 343−351.
Demmel, F., Doster, W., Petry, W., & Schulte, A. (1997) *Eur. Biophys. J. 26*, 327−335.
Dlott, D. D., Frauenfelder, H., Langer, P., Roder, H., & Di Iorio, E. E. (1983) *Proc. Natl. Acad. Sci. U.S.A. 80*, 6239−6243.
Doster, W. (1983) *Biophys. Chem. 17*, 97−103.
Doster, W., Beece, D., Bowne, S. F., Di Iorio, E. E., Eisenstein, L., Frauenfelder, H., Reinisch, L., Shyamsunder, E., Winterhalter, K. H., & Yue, K. T. (1982) *Biochemistry 21*, 4831−4839.
Doster, W., Bowne, S., Frauenfelder, H., Reinisch, L., & Shyamsunder, E. (1987) *J. Mol. Biol. 194*, 299−312.
Doster, W., Kleinert, T., Post, F., & Settles, M. (1995) in *Protein−Solvent Interactions* (Gregory, R. B., Ed.) pp 375−384, Marcel Dekker, New York.
Douzou, P. (1977) *Cryobiochemistry: An Introduction*, Academic Press, London.
Frauenfelder, H. (1997) in *Physics of Biological Systems* (Flyvbjerg, H., Hertz, J., Jensen, M. H., Mouritsen, O. G., & Sneppen, K., Eds.) pp 29−60, Springer−Verlag, Berlin.
Frauenfelder, H., Petsko, G., & Tsernoglou, D. (1979) *Nature 280*, 558−563.
Gavish, B. (1980) *Phys. Rev. Lett. 44*, 1160−1163.
Gavish, B., & Werber, M. (1979) *Biochemistry 18*, 1269−1275.
Gavish, B., & Yedgar, S. (1995) in *Protein−Solvent Interactions* (Gregory, R. B., Ed.) pp 343−373, Marcel Dekker, New York.
Goldanskii, V. I., & Krupyanskii, Y. F. (1995) in *Protein−Solvent Interactions* (Gregory, R. B., Ed.) pp 289−326, Marcel Dekker, New York.
Gottfried, D. S., Peterson, E. S., Sheikh, A. G., Wang, J., Yang, M., & Friedman, J. M. (1996) *J. Phys. Chem. 100*, 12034−12042.
Hagen, S. J., Hofrichter, J., & Eaton, W. A. (1995) *Science 269*, 959−966.
Hagen, S. J., Hofrichter, J., & Eaton, W. A. (1996) *J. Phys. Chem. 100*, 12008−12021.
Hallbrucker, A., Mayer, E., & Johari, G. P. (1989) *Philos. Mag. 60B*, 179−187.
Hartmann, H., Zinser, S., Komninos, P., Schneider, R. T., Nienhaus, G. U., & Parak, F. (1996) *Proc. Natl. Acad. Sci. U.S.A. 93*, 7013−7016.
Hasinoff, B. B. (1977) *Arch. Biochem. Biophys. 183*, 176−188.
Hasinoff, B. B. (1981) *Arch. Biochem. Biophys. 201*, 396−402.
Henry, E. R., Sommer, J. H., Hofrichter, J., & Eaton, W. A. (1983) *J. Mol. Biol. 166*, 443−451.
Iben, I. E. T., Braunstein, D., Doster, W., Frauenfelder, H., Hong, M. K., Johnson, J. B., Luck, S., Ormos, P., Schulte, A., Steinbach, P. J., Xie, A., & Young, R. D. (1989) *Phys. Rev. Lett. 62*, 1916−1919.
Johari, G. P., Hallbrucker, A., & Mayer, E. (1987) *Nature 330*, 552−553.
Johnson, J. B., Lamb, D. C., Frauenfelder, H., Müller, J. D., McMahon, B., Nienhaus, G. U., & Young, R. D. (1996) *Biophys. J. 71*, 1563−1573.
Kramers, H. A. (1940) *Physica 7*, 284−304.
Kubo, R. (1957) *J. Phys. Soc. Jpn. 12*, 570.
Kuriyan, J., Wilz, S., Karplus, M., & Petsko, G. A. (1986) *J. Mol. Biol. 192*, 133−154.
Laidler, K. J. (1987) *Reaction Kinetics*, 3rd ed., pp 112−115, Harper and Row Publishers, New York.
Lambright, D. G., Balasubramanian, S., & Boxer, S. G. (1993) *Biochemistry 32*, 10116−10124.
Lavalette, D., & Tetreau, C. (1988) *Eur. J. Biochem. 177*, 97−108.
Li, T., Quillin, M. L., Phillips, G. N., Jr., & Olson, J. S. (1994) *Biochemistry 33*, 1433−1446.
Lin, T. Y., & Timasheff, S. N. (1996) *Protein Sci. 5*, 372−381.
Lindsey, C. P., & Patterson, G. D. (1980) *J. Chem. Phys 73*, 3348−3357.
Mayer, E. (1994) *Biophys. J. 67*, 862−873.
Ng, K., & Rosenberg, A. (1991) *Biophys. Chem. 39*, 57−68.
Nienhaus, G. U., Mourant, J. R., Chu, K., & Frauenfelder, H. (1994) *Biochemistry 33*, 13413−13430.
Nikolski, B. P. (1959) *Handbuch des Chemikers Vol. 3*, VEB Verlag Technik, Berlin.
Noyes, R. M. (1961) *Prog. React. Kinet. 1*, 129−160.
Parak, F., Knapp, E. W., & Kucheida, D. (1982) *J. Mol. Biol. 161*, 177−194.
Perutz, M. F. (1989) *Trends Biochem. Sci. 14*, 42−44.
Phillips, S. E. V. (1980) *J. Mol. Biol. 142*, 531−554.
Post, F. (1994) Ph.D. Thesis, Technische Universität München.
Post, F., Doster, W., Karvounis, G., & Settles, M. (1993) *Biophys. J. 64*, 1833−1842.
Press, W. H., Flannery, B. P., Teukolsky, S. A., & Vetterling, W. T. (1986) *Numerical Recipes*, Cambridge University Press, Cambridge.
Quillin, M. L., Arduini, R. M., Olson, J. S., & Phillips, G. N., Jr. (1993) *J. Mol. Biol. 243*, 140−155.
Quillin, M. L., Li, T., Olson, J. S., Phillips, G. N., Jr., Dou, Y., Ikeda-Saito, M., Regan, R., Carlson, M., Gibson, Q. H., Li, H., & Elber, R. (1995) *J. Mol. Biol. 245*, 416−436.
Rand, R. P. (1992) *Science 256*, 618.
Rand, R. P., Fuller, N. L., Butko, P., Francis, G., & Nicholls, P. (1993) *Biochemistry 32*, 5924−5929.
Ringe, D., Petsko, G., Kerr, D. E., & de Montellano, P. R. O. (1984) *Biochemistry 23*, 2−4.
Rohlfs, R. J., Mathews, A. J., Carver, T. E., Olson, J. S., Springer, B. A., Egeberg, K. D., & Sligar, S. G. (1990) *J. Biol. Chem. 265*, 3168−3176.
Rosenberg, A., Ng, K., & Punyiczki, M. (1989) *J. Mol. Liq. 42*, 31−43.
Sage, J. T., Schomaker, K. T., & Champion, P. M. (1995) *J. Phys. Chem. 99*, 3394−3405.
Sartor, G., Mayer, E., & Johari, G. P. (1994) *Biophys. J. 66*, 249−258.
Scherer, G. W. (1986) *Relaxation in Glasses and Composites*, Wiley, New York.
Schlichting, I., Berendzen, J., Phillips, G. N., Jr., & Sweet, R. M. (1994) *Nature 317*, 808−812.
Schlitter, J. (1988) *Chem. Phys. 120*, 187−197.
Schofield, P. (1966) *Proc. Phys. Soc. 88*, 149−183.

Settles, M., Post, F., Müller, D., Schulte, A., & Doster, W. (1992) *Biophys. Chem. 43*, 107−116.
Smerdon, S. J., Dodson, G. G., Wilkinson, A. J., Gibson, Q. H., Blackmore, R. S., Carver, T. E., & Olson, J. S. (1991) *Biochemistry 30*, 6252−6260.
Srajer, V., & Champion, P. M. (1991) *Biochemistry 30*, 7390−7402.
Srajer, V., Reinisch, L., & Champion, P. M. (1988) *J. Am. Chem. Soc. 110*, 6656−6670.
Srajer, V., Teng, T., Pradervand, C., Ren, Z., Adachi, S., Schildkamp, W., Bourgeois, D., Wulff, M., & Moffat, K. (1996) *Science 274*, 1726−1729.
Steinbach, P. J. (1996) *Biophys. J. 70*, 1521−1528.
Steinbach, P. J., Ansari, A., Berendzen, J., Braunstein, D., Chu, K., Cowen, B. R., Ehrenstein, D., Frauenfelder, H., Johnson, J. B., Lamb, D. C., Luck, S., Mourant, J. R., Nienhaus, G. U., Ormos, P., Philipp, R., Xie, A., & Young, R. D. (1991) *Biochemistry 30*, 3988−4001.
Steinbach, P. J., Chu, K., Frauenfelder, H., Johnson, J. B., Lamb, D. C., Nienhaus, G. U., Sauke, T. B., & Young, R. D. (1992) *Biophys. J. 61*, 235−245.
Steinhoff, H. J. (1990) *Eur. Biophys. J. 18*, 57−62.
Sun, W. Q., Leopold, A. C., Crowe, L. M., & Crowe, J. H. (1996) *Biophys. J. 70*, 1769−1776.
Takano, T. (1977) *J. Mol. Biol. 110*, 569−584.
Tian, W. D., Sage, J. T., Srajer, V., & Champion, P. M. (1992) *Phys. Rev. Lett. 68*, 408−411.
Tian, W. D., Sage, J. T., Champion, P. M., Chien, E., & Sligar, S. G. (1996) *Biochemistry 35*, 3487−3502.
Timasheff, S. N. (1993) *Annu. Rev. Biophys. Biomol. Struct. 22*, 67−97.
Travaglini Allocatelli, C. T., Cutruzzolà, F., Brancaccio, A., Brunori, M., Qin, J., & La Mar, G. N. (1993) *Biochemistry 32*, 6041−6049.
Williams, G., & Watts, D. C. (1970) *Trans. Faraday Soc. 66*, 80−85.
Yang, F., & Phillips, G. N., Jr. (1996) *J. Mol. Biol. 256*, 762−774.
Yedgar, S., Tetreau, C., Gavish, B., & Lavalette, D. (1995) *Biophys. J. 68*, 665−670.
Young, R. D., & Bowne, S. F. (1984) *J. Chem. Phys. 81*, 3730−3737.

BI971508Q